RWTH AACHEN UNIVERSITY

HELMHOLTZ-INSTITUTE FOR BIOMEDICAL ENGINEERING
RWTH AACHEN

CHAIR FOR MEDICAL INFORMATION TECHNOLOGY
Univ.-Prof. Dr.-Ing. Dr. med. Steffen Leonhardt

Neonatal Infrared Thermography Image Processing

Lluis Bayo Catalan

Supervisor: Abbas Khudair Abbas

Version: 2009-05-19

Pauwelsstraße 20
D-52074 Aachen

Telefon: +49 (0)241 80 -23211
Fax: +49 (0)241 80 -82442
E-Mail: medit@hia.rwth-aachen.de

Declaration

I declare to the best of my knowledge and belief that, this assignment is my own work, all sources have been properly acknowledged, and the assignment contains no plagiarism. This material has not been submitted, either in whole or part at this or any other university.

Place, Date	Signature

Acknowledgement

First of all, I would like to express my sincere appreciation to the MedIT chair with its director Professor Dr.-Ing. Dr.med. Steffen Leonhardt for giving me permission to conduct this student research project (master thesis), to do the necessary investigation and to use the institute's facilities. Special thank to Abbas Khudair, M.Sc., for his commitment to this work, reading, correction and his friendly supervision.
My gratitude also go to my parents and, spcial, my brother Joan who helps me in some troubles. Finally, I would also like to thank my friends from Aachen and from Spain who are always there to help me in anything.

Abstract

The temperature changes inside incubator affect the newborns, who are the most delicate patients. The project proposes an innovative method to monitor the skin temperature of the neonates. The temperature monitoring is carried out by a virtual sensor. This virtual sensor is based in an infrared thermal camera that is placed outside the incubator. In order to obtain the infrared radiation through the incubator Plexiglas, an infrared transparent window is required. The experiment carried out was focused on obtaining the transparent properties in the infrared spectral range measurement of this window. On the other hand, the thermal imaging processing is necessary to obtain the thermal information from the infrared imager and to be able to track the region of interest throughout the field of view.

Contents

1. Introduction

The relevant points of this project are infrared (IR) camera settings and calibrations a measurement of an IR thermography material and the IR image processing applied to tracking some regions of interest (ROIs). The IR camera settings and calibrations are modifiable settings of IR camera which help the user to calibrate the IR thermal camera in different situations. The most important settings are below.
The Modulation Transfer Function (MTF) restricts hard changes in the IR image depending on lens system, detectors, processing electronics and displays.
Nyquist limit which is the frequency equal the reverse of twice the spacing between the samplings and Aliasing that is the effect when spatial frequencies are bigger than Nyquist limit. Noise Equivalent Transfer Differential (NETD) is defined as the scene temperature difference that generates a signal equal to the RMS noise. Field of View (FOV) is the angle subtended at the entrance aperture of the lens objective of a thermal imager (camera) by total scene accommodated in the imager display.
The Dynamic range describes the ratio between the smallest and biggest temperature value chosen to transform to the discrete levels, normally 256 levels.
Measurement of an IR thermography material is the study of the Polyethylene foil (PEF) transmittance. To know the PEF properties are carried out six kinds of experiments. Room temperature object shows the PEF behavior with a test object at a 20C. Hot temperature object presents the PEF behavior with a test object between 70C to 85C. IR transparent window PEF 0.1mm versus PEF 0.5mm is the behavior of two windows simultaneously in different distance.
The IR transparent windows versus test objects are the behavior of each window with test objects changing the distances. Hot to environment temperature is the transmittance behavior in cooling down test object. And camera versus environment temperature shows camera temperature behavior versus environment temperature in a long period of time.
IR image processing is the part of the project where it is solved the ROI tracking. The final results of this part are to extract temperature information of newborn ROI, and it is made in real time. This section has five parts. IR Acquisition acquires the IR image from the IR camera and converts to correct format image. ROI geometry definition specifies the shape of the ROI. Tracking Object tracks the ROI in the IR image.
ROI Temperature level extraction converts the color information of isolated ROI to temperature information. And Display shows IR image and tracked ROI and the ROI temperature information.
Before to start the project it is good to know which is the Thermal Balance and Ther-

moregulation of the human body, to know the behavior of human skin in different situation and more to the point of newborns skin temperature. The humans' temperature remains relatively constant despite changes in the environmental temperature. This homeothermy applies only to the core temperature (≈37C) of the body. The extremities skin ("shell") exhibit poikilothermy, i.e., their temperature varies to some extent with environmental temperature.
In order to maintain a constant core temperature, the body must balance the amount of heat it produces and absorbs with the amount loses; this is thermoregulation. To keep warm, the body may have to generate additional voluntary (limb movement) and involuntary (shivering) muscle contractions. Newborns also have tissue known as brown fat, which enables them to produce additional heat without shivering.
Heat produced in the body is absorbed by the bloodstream and conveyed to the body surface. In order for this internal flow of heat to occur, the temperature of the body surface must be lower than that of the body interior. The blood supply to the skin is the chief determinant of heat transport to the skin. Heat loss occurs by the physical processes of radiation, conduction, convection and evaporation [SD09].

- The heat radiates from the body into the environment when no radiating object is present. Heat radiation does not require the aid of any vehicle and hardly affected by the air temperature. Therefore, the body loses heat to a cold wall (despite warm air in between) and absorbs radiation from the sun or an infrared radiator without air or cold air, respectively, in between.

- The conduction and convection involve the transfer of heat from the skin to cooler air or a cooler object in contact with the body (conduction). The amount of heat lost by conduction to air increases greatly when the warmed air moves away from the body by natural convection (heated air rises) or forced convection (wind).

- The first two mechanisms alone are unable to maintain adequate temperature homeostasis at high environmental temperatures or during strenuous physical activity. Evaporation is the means by which the body copes with the additional heat. The water lost by evaporation reaches the skin surface by diffusion (insensible perspiration) and by neuron-activated sweat glands. About 2428 kJ (580 kcal) of heat are lost for each litter of water evaporating and thereby cooling the skin. At temperature above 36C or so, heat loss occurs by evaporation only.

1.1. Motivation

Monitoring newborn incubator temperature control with thermal image can be useful as early diagnostic technique. That will be possible with Infrared camera connected to a computer that making image processing can be extract information about temperature in region of interest (ROI). Therefore, design of a flexible GUI-based image-pattern clustering; was of vital aspect in understanding neonatal thermography process and underlying physiological function.

Initially, infrared recorder that measures a temperature is important to have control about environment temperature. Besides, this case has two environments well differentiated and affect to the IR camera calibration. The two environments are inside incubator and incubators' room. The mainly difference is the temperature in each environment, 36C to 37C and 25C, incubator inside and outside, respectively.

Next step is decided which environment is placed the IR camera. It is easy think that best place to situate the IR camera is inside of incubator, but it has few troubles. Such as humidity inside is higher than humidity that the IR camera works well and IR camera dimensions are big to not disturb nurses' work. For this reason, placing IR camera inside of incubator is dismissed.

In order that IR camera is placed outside incubator, this provokes new different trouble. This new difficulty is that the two environments are among a Plexiglas shell. Plexiglas is a transparent material in the visible frequencies range, but not in the infrared range.

The proposed solution for this trouble is to find a transparent material in infrared range and this material is used like a window instead of Plexiglas between the two environments. Furthermore, other calibration's consideration is the high humidity incubator inside. The high humidity affects in infrared, for this reason high humidity must be calibrated.

1.2. Challenges

Developing of a virtual sensor, which can be able to measure newborn's temperature inside the incubator without contact, this developed contact-less sensor considered as an innovative temperature measurement method [Mer06]. The principal points of this proposed sensor are; contact less, non-invasive and more accurate than the old techniques. Where it was with contact and its precious was 0.5C, however this innovative technique has a precious of 0.01C.

1.3. Literature survey

R. B. Barnes, 1963, [Bar63] researched regarding the thermography imaging of the human body with an infrared-radiant energy that provided new concepts for contact-less temperature monitoring. His research was that using IR energy might be recorded as a thermogram to yield a quantitative temperature map of the skin. If the nude subject had remained quiet in a cool room for 10 to 15 minutes prior to thermography, the skin temperatures were determined largely by the vascularity of the skin itself and by the heat conducted from within the body. Since, under these conditions, the contrasts which appear arise essentially from the internal sources of heat, the resulting thermograms yield information concerning certain pathological conditions within the body.

It was one of the first researches in medicine via infrared performed by R. P. Clark and J. K. Stothers, 1980 [Cla80] where they carried out a neonatal skin temperature distribution measurement; using infrared color thermography; which was the first research dealing with neonatal infrared thermography.

They arrived to results that the upper arm, the thigh and the buttock of newborn have a mean value and that they are responsive to environmental temperature change. They observed that the skin overlying the upper abdomen is hot and relatively insensitive to environmental temperature changes was of clinical significance.

After this, others investigators researched in the field of neonates and Infrared thermography. E. S. Anderson, M. P. Wailoo, S. A. Petersen, 1990,[AP90] researched in use of thermographic imaging to study babies sleeping at home. Body temperature was recorded and thermal imaging carried out on five babies, four of whom slept in conditions similar for ambient temperature and insulation, and who showed similar patterns of deep body temperature and thermal imaging. The other one slept in much hotter conditions, and made a different thermogenic response [Ryl72].

These cases were a testament to the capabilities of infants for thermoregulation, and the possibility of using thermographic imaging at home to show heat loss and sleeping body movements in different home conditions. Although they had reported only two cases, they believed that the babies clearly showed the need to study in much more detail the role of head, hands, and other parts of the body in the thermoregulation of infants under home conditions and the effects of different sleeping positions on temperature control and other physiological systems.

Above all, they confirmed the feasibility of detailed study of babies at home. Another research, A. K. Adams, R. A. Nelson, E. F. Bell, and C. A. Egoavil, 1999, [Ada00] realized the use of infrared thermographic calorimetry to determine energy expenditure in preterm

infants. The objective of their study was to validate in infants a newly developed method of determining energy expenditure, infrared thermographic calorimetry (ITC), against an established method, respiratory indirect calorimetry (IC).
ITC measures mean infant body surface temperature. ITC was used in conjunction with heat loss theory to calculate radiant, convective, evaporative, and conductive heat losses and thereby determine total energy expenditure.
The conclusion that they extracted was that ITC was an accurate, noninvasive method for measurement of heat loss and energy expenditure in healthy preterm infants, and therefore it might be a useful clinical and research tool. And other interesting research, I. Christidisa, H. Zottera, H. Roseggerb, H. Engeleb, R. Kurza and R. Kerbla, 2002, [Chr03] carried out Infrared Thermography in Newborns: The First Hour after Birth.
The title reflects the aim of their study to investigate the surface temperature in newborns within the first hour after delivery. Furthermore, the influence of different environmental conditions with regard to surface temperature was documented. Their investigations demonstrated that infrared thermography is an easily applicable tool to describe the temperature profile of individuals.
Without the need of direct skin contact, it might be helpful for optimizing the environmental conditions at delivery suites and neonatal intensive-care units (NICU). Although, the method lacked information about core temperature, it might be helpful to optimize environmental conditions in neonatal care and especially at delivery units.

1.4. Scope of the project

subsequently, the introduction, in the next chapter is a brief history and properties of infrared thermal imaging and infrared camera technologies, settings and calibration. In the third chapter shows results obtained in experiments about transparency properties for different material in infrared frequency range, on different situations. The following chapter, the fourth, present which method of image processing is used to achieve the tracking ROI inside image. In chapter 5 it is exposed some discussions and conclusion about this project. And chapter 6 is proposed some future work.

2. Infrared Thermography Imaging

In the late seventeenth and early eighteenth century, Huygens, Roemer and Fahrenheit all proposed the need for calibrate scale. Celsius proposed a centigrade scale based on ice and boiling water. He strangely suggested that boiling water should be zero and melting ice 100 on his scale.

It was the Danish biologist Linnaeus in 1750 who proposed the reversal of Celsius scale, as it is known today. Although International Standards have given the term Celsius to the 0 to 100 scale today, strictly speaking it would be historically accurate to refer to degrees Linnaeus or centigrade. The Clinical thermometer, which has been universally used in medicine for over 130 years, was developed by Dr. Carl Wunderlich in 1868.

Heat transfer by radiation occurs in the infrared spectrum, which can be imager by electronic thermal imaging. Infrared radiation was discovered in 1800 when Sir William Herschel performed his famous experiment to measure heat beyond the visible spectrum.

William Herschel showed that was a (dark heat) present. Furthermore, he observed that they were reflected, refracted, absorbed and transmitted in a similar form to visible light. John Herschel, William's son, repeated some experiments after his father's death, and successfully made an image using solar radiation. This he called a "thermogram", a term still in use today to describe an image made by thermal radiation.

A major development came in the early 1940s with the first electronic sensor for infrared radiation. Rudimentary night vision systems were produced toward the end of the Second World War for use by snipers. The electrons from near-infrared cathodes were directed onto visible phosphors which converted the infrared to the visible light. Sniper scope devices, based on this principle, were provided for soldiers in the Pacific in the 1945.

Approximately at the same time, another device was made from indium antimonide; this was mounted at the base of small Dewar vessel to allow cooling with liquid nitrogen. A cumbersome device such as this, which required a constant supply of liquid nitrogen, was clearly impractical for battlefield use but could be used with only minor inconvenience in a hospital. The first medical images taken with a British prototype system, the (Pyroscan), were made at The Middlesex Hospital in London and The Royal National Hospital for Rheumatic Diseases in Bath between 1959 and 1961.

In the meantime, the cascade image tube, which had been pioneered during World War II in Germany, had been developed by RCA into a multi-alkali photo-cathode tube whose performance exceeded expectations. These strides in technology were motivated by military needs in Vietnam; they were classified and, therefore, unavailable to clinicians. However, a mark 2 Pyroscan was made for medical use in 1962, with improved images.

The mechanical scanning was slow and each image needed from 2 to 5 minutes to record. The final picture was written line by line on electro-sensitive paper. In the seventies, the U.S. Military sponsored the development of a multi-element detector array that was to form the basis of the real-time framing imager. This led to the targeting and navigation system known as Forward Looking Infrared (FLIR) systems which had the added advantage of being able to detect warm objects through smoke and fog.

During this time the potential for thermal imaging in medicine was being explored in an increasing number of centers. Earlier work by the American physiologist J. Hardy had shown that the human skin, regardless of color, is a highly efficient radiator with an emissivity of 0.98 which is close to that of a perfect black body. Even so, the normal temperature of skin in the region of 20 to 30C generated low intensities of infrared radiation at about 10 μm wavelengths. The detection of such low intensities at these wavelengths presented a considerable challenge to the technology of the day.

By mid-seventies, computer technology made a widespread impact with the introduction of smaller mini and microcomputers at affordable prices. In Bath, a special system for nuclear medicine made in Sweden was adapted for thermal imaging. A color screen was provided to display the digitized image. With computerization many problems began to be solved.

The images were archived in digital form, standard regions of interest could be selected, and temperature measurements obtained from images. Manufacturers of thermal imaging equipment slowly adapted to the call for quantification and some sold thermal radiation calibration sources to their customers to aid the standardization technique.

Workshops that had started in the late 1960s became a regular feature, and the European Thermographic Association was formed with a major conference in Amsterdam in 1974.

Apart from a range of physiological and medical applications groups were formed to formulate guidelines for good practice. This included the requirements for patient preparation, conditions for thermal imaging and criteria for the use of thermal imaging in medicine and pharmacology.

With the end of the cold war, the greatly improved military technology was declassified and its use for the medical applications was encouraged. Consequently, the first focal plane array detectors came from the multi-element arrays, with increasing numbers of pixel/elements, yielding high resolution at video frame rates.

The uncooled bolometer arrays have also been shown to be adequate for many medical applications. Without the need for electronic cooling systems these cameras are almost maintenance free. Good software with enhancement and analyses is now expected in thermal imaging.

Many commercial systems use general imaging software, which is primarily designed for

industrial users of the technique. A few dedicated medical software packages have been produced, which can even enhance the images from the older cameras. As standardization of image capture and analysis becomes more widely accepted, the ability to manage the image and, if necessary, to transmit them over an intranet or internet for communication becomes paramount[RJ08, Jia05].
The modern thermal imaging systems are already digital and quantifiable, and ready for the integration into anticipated hospital and clinical computer networks.

2.1. Infrared Thermography Physical Principles

The electromagnetic spectrum is the range frequencies of electromagnetic radiation in present day. This spectrum is divided, lowest wavelength to highest wavelength and its range, in Gamma rays (<10pm), X-rays (<10nm), Ultraviolet (<380nm), Visible (<780nm), Infrared (<1mm), Microwaves (<30cm) and Radio waves (<10 km, 30 kHz). All of these radiations emit energy that is described by frequency or wavelength.

$$E = h \cdot f; E = h \cdot \frac{c}{\lambda} \tag{2.1}$$

Where h; is the Plank's constant and its value is 6.2310^{-34} Js.
Figure 2.1 represents the electromagnetic spectrum that is divided in different frequency range. Visual and Infrared ranges are amplified at bottom of the image. The gamma (γ) rays were discovered by Paul Villard in 1900 and are electromagnetic radiation of high energy [Ger99]. They are useful to astronomers in the study of high energy regions and are produced in nuclear reactions. X-rays were discovered by Wilhelm Conrad Rntgen in 1895. There principal use who everybody knows is radiography [Mou95]. This is used to 'see through' objects. Ultraviolet (UV) were discovered by Johan Wilhelm Ritter in 1801 [Wil03]. UV is found in sunlight and can break chemical bonds, makings molecules unusually reactive or ionizing them. UV radiation can cause sunburn and some forms of skin cancer. Visible radiation is the range of frequencies that the human eyes are sensitive and are divided in color palette. Infrared radiation is the electromagnetic range spectrum that we are interested and we have more exhaustive explanation after this electromagnetic introduction. Microwaves that the first use this word was Robert Dicke [MP50] in 1946 are used in many applications like communication, navigation, remote sensing and spectroscopy, these are few possible applications. And Radio waves are utilized in old communications. Inside this frequency range, the more exactly frequencies lies between 20 Hz-20 kHz, are the human hearing sensitivity

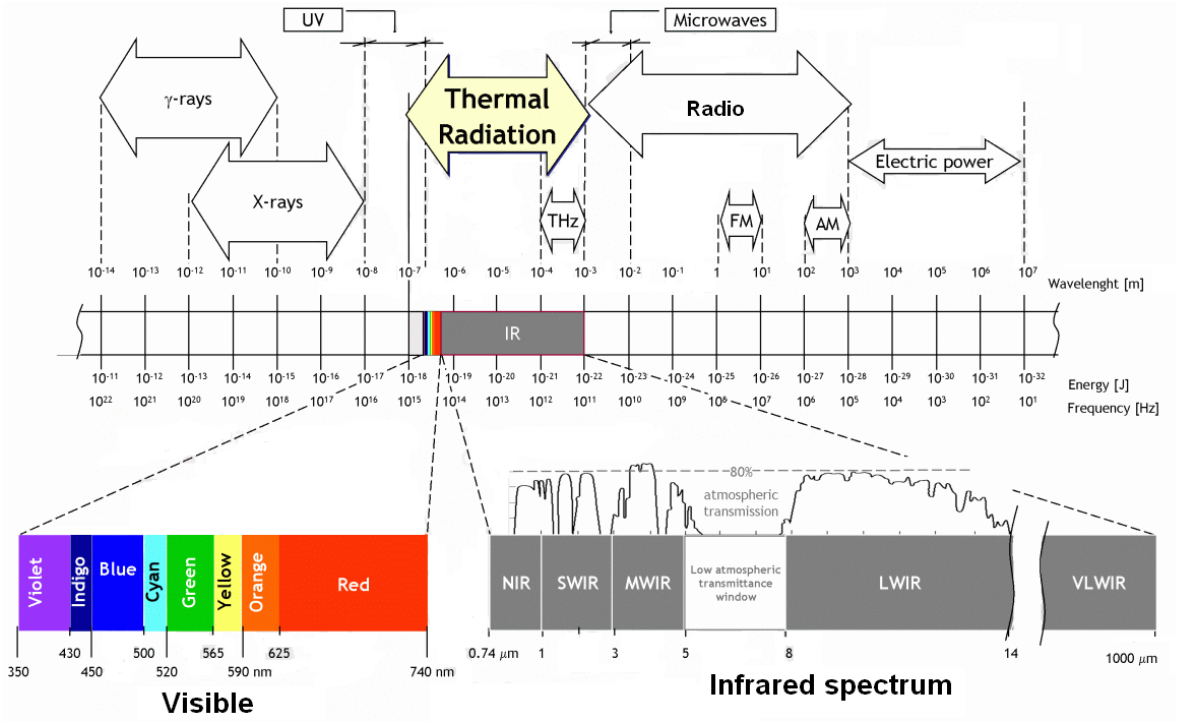

Figure 2.1: Spectrum of electromagnetic(EM)waves with a specified subdivision of infrared spectral bandwidth

2.1.1. Infrared radiation

The discovery of infrared radiation is ascribed to Frederick William Herschel in the early nineteenth century. He observed that each color light had individual temperature. After this, Herschel decided to measure the temperature beyond the red light. He found that this region had higher temperatures than others. He named this radiation “calorific rays“. He observed that they were reflected, refracted, absorbed and transmitted in a similar form to visible light [Hin09].

The infrared band for a sensor response division scheme is normally divided in Near-Wave Infrared (NWIR; 0.74 - 1μm), Short-Wave Infrared (SWIR; 1-3μm), Middle-Wave Infrared (MWIR; 3-5μm) and Long-Wave Infrared (LWIR; 8-14μm). Band between 5μm to 8μm is named Low atmospheric transmittance window because the light suffers highest attenuation in this band, as seen in Figure 2.2.

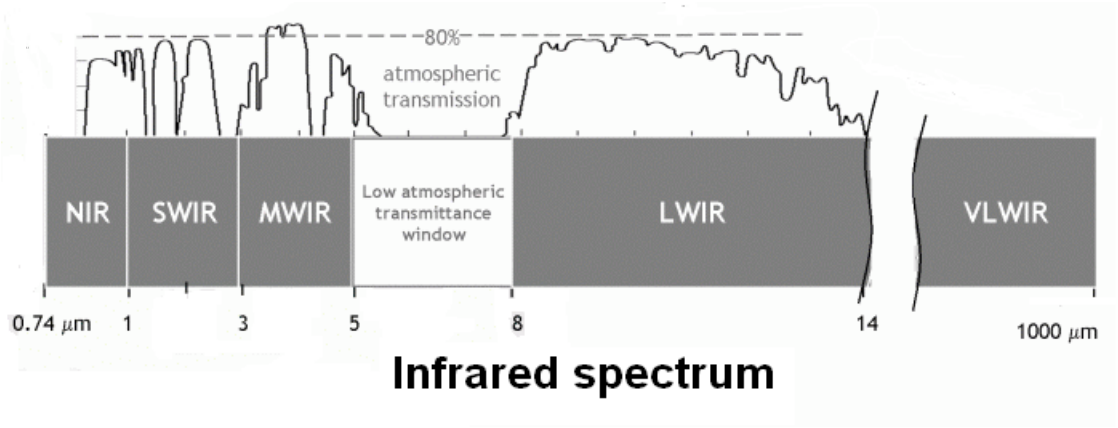

Figure 2.2: Infrared spectrum with atmospheric transmittance.

2.1.2. Plank's Equation

The Plank's equation describes temperature and surface emissivity for a particular wavelength that is the maximum radiation energy that can be emitted by body a given wavelength. This equation can be written as:

$$W(\lambda,T)e(\lambda)\frac{c_1}{\pi\lambda^5 e^{\frac{c_2}{\lambda T}}-1}W/cm^2\cdot\mu m$$

where $W(\lambda,T)$ is the radiance for a wavelength, λ, in μm and a temperature, T, in Kelvin. The units of the radiance is $watts m^{-2} stereoradians^{-1}\mu m^{-1}$ and c_1 and c_2 are a constants of $c_1 = 3.7418104 W\mu m^4/cm^2$ and $c_2 = 1.4388104\mu mK$, respectively. The emissivity, $e(\lambda)$, varies in the range 0 to 1, depends by body and wavelength, . Black body for a range of wavelength is when the emissivity in this range are approximately 1, $e(\lambda) \approx 1$. They are used as standard source of a radiation for calibration purposes [GP08, Wil09]. Blackbodies are carefully designed, heated or cooled cavities that have an exit aperture with a radiant transmittance that is given to a very close approximation by Planck's equation where the effective emissivity is unity. The radiance of the blackbody is calculated from a knowledge of its temperature-hence the importance of having calibrated temperature sensors. The theoretical concept for a blackbody is that the walls of the cavity will themselves have a high emissivity, but that the effective emissivity is increased because the design of the cavity ensures that any radiation emitted by the cavity has undergone several reflections off the cavity walls. For this reason, it is important that the walls of the cavity are at the same uniform temperature and that this is the temperature indicated by the temperature

sensor(s).

2.2. Infrared (IR) camera

The principals' elements of thermal imager are [Wil09]:

- An optical system that can form an image using radiation in the thermal wavelength range.
- One or more detector elements that can convert the thermal radiation into electrical signals proportional to the radiation falling on them.
- Some systems require a scanning mechanism that scans the field of view of the imager, although most modern imagers do not require this; since they use large detector arrays that completely cover the field of view of the imager.
- An electronic processor that can convert electrical signal into a video signal.
- A display unit that generates a visual image from the video signal.

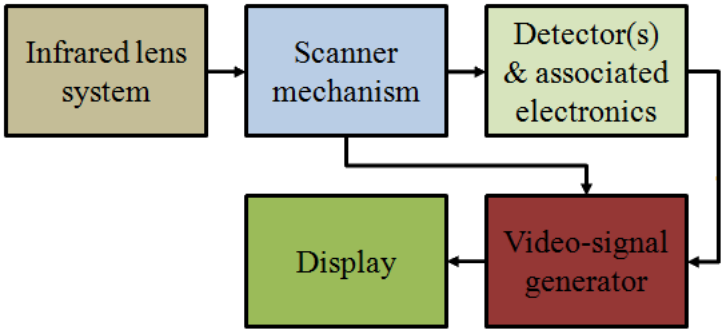

Figure 2.3: Diagram block of the signal process in IR camera.

The schema from Figure 2.3 shows the process that Infrared signal makes since optical system to displayer.

Optical System

The design of optical systems used in thermal imagers is in the same way as optical systems for visible wavelengths. The main difference is the materials used in visual wavelength are different. And in fact, the optical materials used in the 3 - 5 m band or in the 8 - 14 m band are different too [Klo91].

Thermal Detectors

The thermal detector or thermal detector array is possibly the most important part of a thermal imager. It largely determines the potential level of thermal and spatial resolution that can be achieved as well as the complexity that is required to realize this potential. There are basically two types of thermal infrared (IR) detectors. The first depends on the IR radiation heating the detector element, with the resulting temperature rise then triggering some other physical mechanism that is taken as a measure of the radiation falling on the element. This type of detector is generally known as a thermal detector.

The second detector type is one where the photons, which are the incident radiation, interact at atomic or molecular level with the material of the detector, to produce charge carriers that generate a voltage across the detector element or a change in its electrical resistance. The mechanism usually involves an electron absorbing a photon and, as a result, moving from one quantum energy level to another. This type of detector is usually referred to as a photon or quantum detector [HR02, **?**].

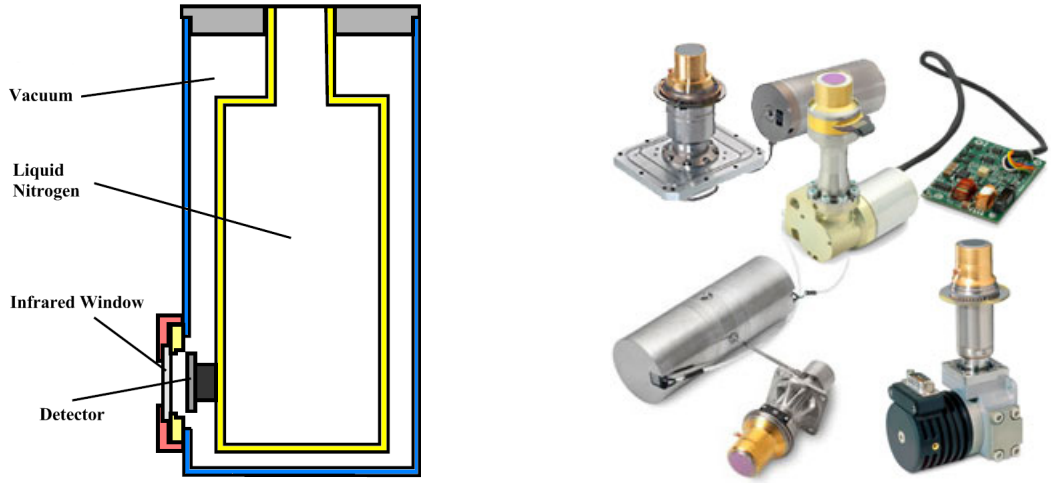

Figure 2.4: Cooled IR detector and commercial examples.

Figure 2.4 presents a schema which explains the different parts that cooled IR detector has and couple of commercial cooled IR detectors.

Image resolution	Pitch (μm)	Pricipals	IR Detector material	geometric MTF (mm^{-1})	Manufacturer
1 x 128	100	pyroelectric	LiTaO	0.6 to 3	DIAS Dresden
328 x 245	48.5	pyroelectric	BaSrTi	0.6 to 5	Texas Instruments (TI)
100 x 100	100	pyroelectric	PbSkTa	0.8 to 3	GEC Marconi
384 x 288	40	pyroelectric	PbSkTa	0.8 to 5	GEC Marconi
336 x 240	50	Bolometer	VOx	0.9 to 5	Honeywell
327 x 245	46	Bolometer	VOx	0.9 to 5	Loral
128 x 128	100	Bolometer	p/n-Poly-Si	0.9 to 3	NEC
320 x 240	50	Micro-cantilaver	Bimetall TiWaufSiC	0.8 to 5	Sarcon Micro-system

Table 2.1: Some typical IR detectors.

Table 2.1 shows different kind of detectors used nowadays. It has image resolution, pitch, principals of detection, IR detector material, geometric MTF and the manufacturer of the detector, that information is useful in selecting the type of detector use un a IR thermal imager, as the follow factors to consider:

- The wavelength band in which it responds

- The frequency response

- The thermal sensitivity and spatial resolution that can be achieved

- Cooling requirements and the associated complexity, cost, and possible inconvenience

- Reliability and cost

Scanning Mechanism

The function of a scanning mechanism is to move the image formed by the lens system over the detector element(s) in a well-controlled fashion. Scanner systems normally fall into one of three classes as represented by the one-dimensional (1D) oscillating mirror scanner arrangements. In the first of these the scanner occupies the space between the image-forming optical system and the detector. In the next arrangement the scanner is between the external object and the image-forming optical system, and in the third arrangement the scanner is placed between a focal front end and the image-forming back end of the optical system [Can99].

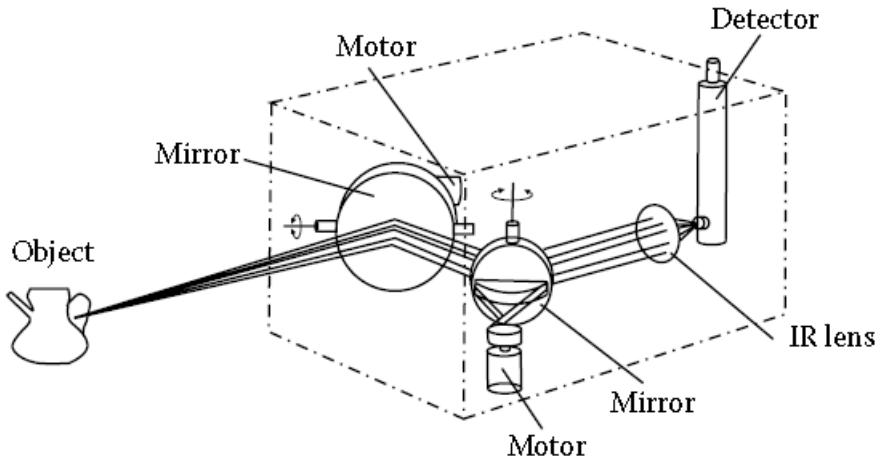

Figure 2.5: Scanning Mechanism.

One kind of mechanisms to scan the IR image is shown in Figure 2.5. Figure 2.5 is a schema where it is to be seen two mirrors with its respective motors and IR lands with detector at the bottom of image. The mirrors with motor are used to scan all FOV. Left mirror scans the vertical axis and the right mirror scans the horizontal axis, this is one way that IR cameras with single IR detector scan FOV.

Special Signal Processing

The thermal image produced by the optical system will in general consist of a very high average background level of radiation corresponding approximately to the radiation emitted by a surface that is at ambient temperature, together with relatively small departures from this average level that represent the temperature and emissivity differences between the objects in the scene. So, for example, the difference in the radiation received from a surface at 18C and one at 22C in the 8-12 m band is only 7% of the total (background) radiation in the same band from a surface at 20C. The signal of interest in generating the video signal for the camera output is that corresponding to this difference and not the absolute addition level [GC94].

To carry out a pseudo-color image from the camera, the IR signal is processed in different steps, as shown in Figure 2.6. First, the signal is converted from analog to digital. Second step is compensating for clamping offset. Third one compensates for unit-radiation by camera. The fourth predicts the temperature knowing emission degree, air humidity, air temperature and distance, the calibration parameters. In the fifth step it is setting the radiation temperature. And the last step before display, it is selected the temperature range and

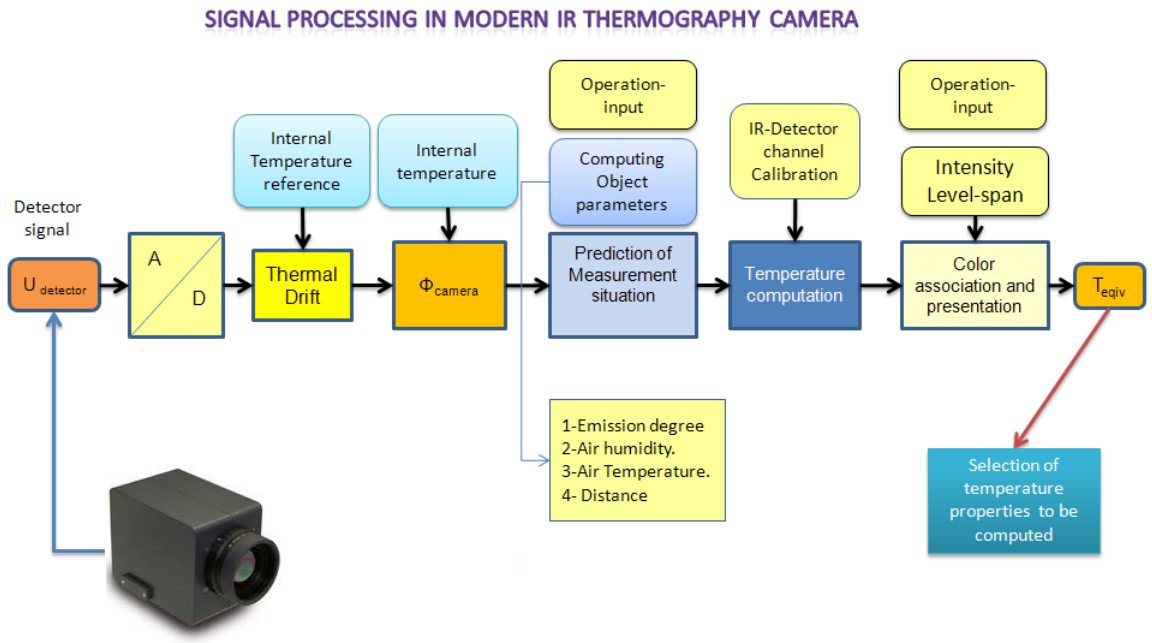

Figure 2.6: Signal processing in modern IR thermography camera.

pseudo-color.

Displays

The image generated by a thermal imager is normally viewed on either a separate external display that could be a computer screen or a small display that forms part of the camera and is designed to be looked at directly or through an eyepiece. The small, flat-screen, direct-view displays that are part of a camera are usually liquid crystal displays (LCDs). LCDs are also frequently used in eyepiece displays. Displays can be monochromatic or color. In the latter case, images can be color coded to show temperature differences as color differences.

2.3. Settings and Calibration

2.3.1. Modulation Transfer Function (MTF)

The MTF of the complete imager is the product of the MTFs of the lens system, the detector, the processing electronics, and displays.

The MTF of the lens is the ratio of the contrast in the image of the sinewave grating to the

contrast in the original object,

$$MTF = \frac{ImageContrast}{ObjectContrast} \tag{2.3}$$

The contrast is defined as

$$Contrast = \frac{I_{max} - I_{min}}{I_{max} + I_{min}} \tag{2.4}$$

And where I_{max} and I_{min} are the maximum and the minimum intensity in the sinewave, respectively. The Figure 2.7 shows the measurement of the MTF.

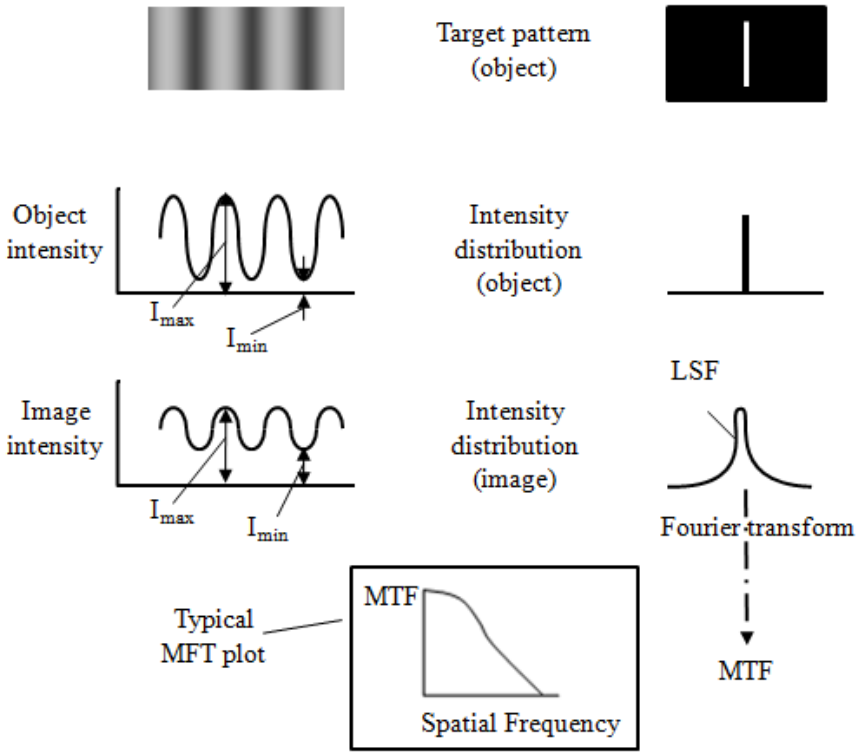

Figure 2.7: Scheme of how Lens MTF is defined and measured.

The exposed stages in Figure 2.7 explains how are measured the lens MTF. From top to bottom, first is shown the original image, a sinewave is target pattern. Second is the real representation of the target pattern intensity and its intensity distribution in spatial frequency domain which is a perfect frequency component. Third is the captured representation of the object intensity and its intensity distribution which is not a perfect frequency component. The ratio between third and second stage are the MTF that is represented in the spatial frequency domain as seen in the square of the Figure 7 and represents a low pass filter.

The MTF of detector is the ratio of the modulation of the output signal to the modulation of a radiant flux input that is a spatially varying 1D sinewave that is traversed across the detector [Wil98].
For a rectangular or square detector with a width w in the scan direction and a uniform response over its area, the MTF is given by

$$MTF(s) = \left| \frac{sin(\pi \cdot w \cdot s)}{\pi \cdot w \cdot s} \right| \tag{2.5}$$

Where s is spatial frequency in cycle/mm when w is measured in millimeters.

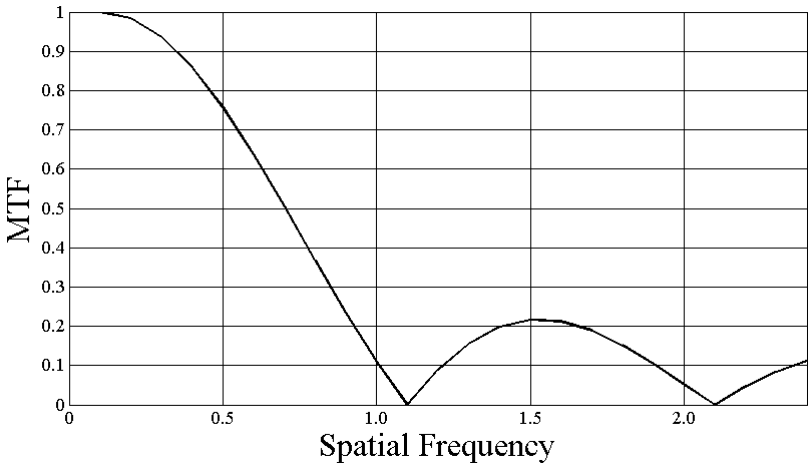

Figure 2.8: Graphic representation of square detector MTF.

Figure 2.8 is Equation 2.6 representation that is a kind of detector MTF represented in the spatial frequency domain. And as the lens MTF, detector MTF typifies a low pass filter. The MTF of the display is a measure of the quality of the image that the display can generate, in the sense of reproducing image detail with good contrast.
The slow response of a display can reduce the effective MTF for moving objects. The relevant MTF is normally referred to as the DMTF (Dynamic-MTF) and if this is likely to be the problem, it can be assessed by measuring the response or decay time of the display [Wil98]. The MTF will in general vary with target orientation and with position in the field of view, and the kind of lens; it is usual to measure the MTF for radial and tangential orientations and for two or more field positions either side of the axis as well as on-axis.

As seen in Figure 2.9, the product of all MTF of different parts of thermal imager is the final MTF in spatial frequency domain. As all individual MTF are a low pass filter the response

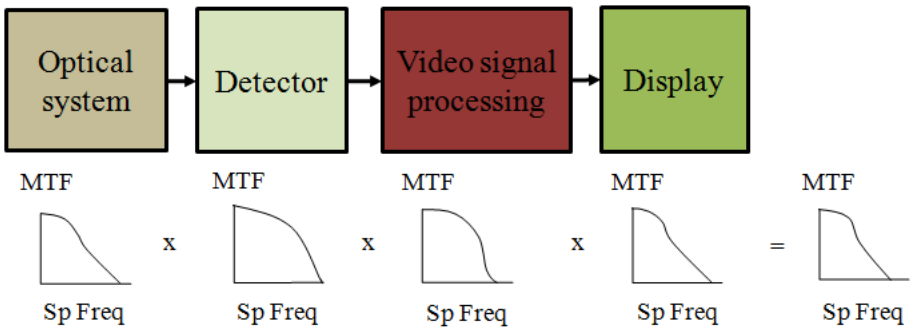

Figure 2.9: Final MTF of thermal imager.

of final MTF is also a low pass filter [GDH07].

2.3.2. Nyquist limit and Aliasing

The Nyquist limit is the frequency corresponding to a period equal to half the spacing of the sampling points, as equation shows,

$$NyquistFrequency = S_{Nyq} = \frac{1}{2 \cdot p} \tag{2.6}$$

Where p is the distances between sampling points. Aliasing happens when and where the scene contains spatial frequencies greater than the Nyquist limit, and when the combined MTF of the optical system and the detectors is greater than zero at spatial frequencies above the Nyquist limit [23].

2.3.3. Noise Equivalent Temperature Differential (NETD)

In general, imager sensitivity is a measure of the measure of the smallest signal that is detectable by a sensor. For IR imaging systems, noise equivalent temperature difference (NETD) is a measure of sensitivity. Sensitivity is determined using the principles of radiometry and characteristics of the detector. The system intensity transfer function (SITF) can be used to estimate the noise equivalent temperature difference. The NETD parameter can be defined as the system noise root meas square (rms) voltage over the noise differential output. It is the smallest measurable signal produced by a large target (extended source), in other words the minimum measurable signal.
Equation below describes NETD as a function of noise voltage and the system intensity

transfer function. The measured NETD values are determined from a line of video stripped from image of s test target, as depicted in Figure 4.10. A square test target is placed before a black body source. The ΔT is the difference between the black body temperature and the mask. This target is then placed at the focal point of an off axis parabolic mirror. The mirror serves for propose of a long optical path length to the target, yet relieves the tester from concerns over atmospheric losses to the temperature difference. The SITF slope for the scan line is the $\Delta\Sigma/\Delta T$, where $\Delta\Sigma$ is signal measured for a given ΔT. The N_{rms} is the background signal on the same line.

$$NETD = \frac{N_{rms}[volts]}{SITF_{Slope}[\frac{volts}{K}]} \tag{2.7}$$

After calculating both the temporal and spatial noise, a signal transfer function (SiTF) is measured. The field of view of the camera is again flooded with a uniform temperature source. The temperature of the source is varied over the dynamic range of the camera's output while the mean array voltage response is recorded. The slope of the resulting curve yields the SiTF responsivity in volt per degree Kelvin change in the scene temperature. Once both the SiTF curve and the temporal and spatial noise in volts are known, the NETD can be calculated. This is accomplished by dividing the temporal and spatial noise in volts by the responsivity in volts per degree Kelvin. The resulting NETD values represent the minimum discernable change in scene temperature for both spatial and the temporal observation [LA03].

2.3.4. Field of View (FOV)

The FOV is the angle subtended at the entrance aperture of the lens objective of a thermal imager by the total scene accommodated in the imager display. There will be a value for the horizontal FOV and the vertical FOV, although this is expressed as the horizontal FOV together with the image aspect ratio [Dan06].

$$FOV = 2 \cdot tan^{-1}\left(\frac{arraydimension}{2 \cdot focallens}\right) \tag{2.8}$$

2.3.5. Dynamic Range

The responsivity function also provides dynamic range linearity information. The camera dynamic range is the maximum measurable input signal divided by the minimum measurable

signal. NETD is assumed to be the minimum measurable signal. Depending upon the application, the maximum input value may be defined by one of several methods.
For the most systems, the detector output signal is adjusted both in gain and offset so that the dynamic range of the A/D converter is maximized. The converter can handle an input signal between 0 and 1 volt and an output between 0 and 255 counts. By selecting the gain and offset, any detector voltage range can be mapped into the digital output. Figure 2.10 shows 3 different system gains and offsets. When the source flux level is less than ϕ_{min}, the source will not be seen (i.e., it will appear as 0 counts). When the flux level is greater than ϕ_{max}, the source will appear as 255 counts, and the system is said to be saturated. The gain parameters, ϕ_{min} and ϕ_{max}, are redefined for each gain offset level setting, as seen in Figure 2.10.

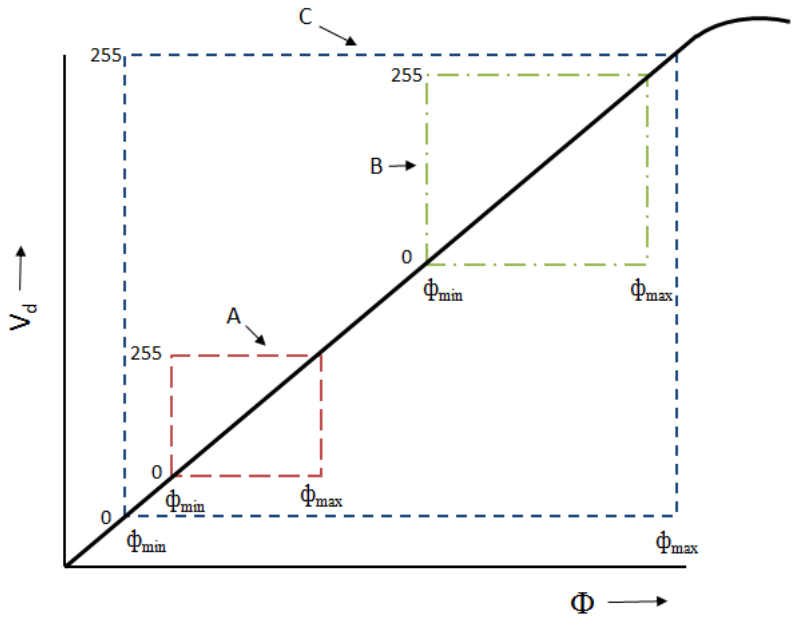

Figure 2.10: Different gains and voltage offsets affect the input-to-output.

In Figure 2.10, Output A below occurs with maximum gain, red square. Point B occurs with moderate gain, green square, and C with minimum gain, blue square. For the various gains, the detector output gets mapped into the full dynamic range of the A/D converter [GP08].

3. Infrared thermography calibartion

In this chapter it is explained in details, the methods and the results of the infrared (IR) thermography calibration procedures. The investigation will be focused on the transparent windows properties in infrared spectral range measurement. Moreover, it will be a brief explanation about the software-setting and the graphical user interface used to capture IR image from the thermal (IR) camera, IRBIS-3 Professional platform. The IR transparent measurements are carried out to know the IR transparent properties of material that replace a piece of Plexiglas in incubator shell, previously mentioned in chapter 2. At the end of the chapter it proposed some discussions about it.
The selection of the IR transparent material which replaces the Plexiglas is a Polyethylene Foil (PEF) with two different widths, 0.1 and 0.5mm. Two PE bottles filled with water are the test objects. These test objects are situated one meter from the camera in the other end of the guide. The experiment consists of changing the (window-object) distance and (window-camera) distance. In addition; to warming up the water inside one test object until boiling point, approximately 85C.

3.1. Experiment equipment

The objective of these experiments; is to find the infrared (IR) transmittance characteristics of the windows material made of plastic polyethylene (PE). This information is used to calibrate the camera in order to obtain the real temperature. Figure 3.1 shows the situation of the experiment equipment:

Figure 3.1: General setup of infrared thermography calibration measurement experiment.

Figure 3.1 display the general setup of thermography measurement equipment in the work-bench to realize a measurement. It recognizes the connected laptop to IR camera, IR camera at right is placed with tripod, a fixed guide and test object and IR transparent window are ready to realize the measurement in them place.

Figure 3.2: IR camera and guide-ruler settings for IR thermography calibration experiments.

A one meter ruler is used as device of measuring distance and guide for windows and test objects in the experiments. It is necessary to build a guide in order to move the windows along the guide. In the ruler all along brackets are attached in order to increase high and

be used as guides for the windows. Next, the guide-ruler is fixed at the workbench. Fixed guide-ruler and IR camera are placed as seen in Figure 3.2. The IR camera lens is situated at 0 cm point of the guide-ruler.

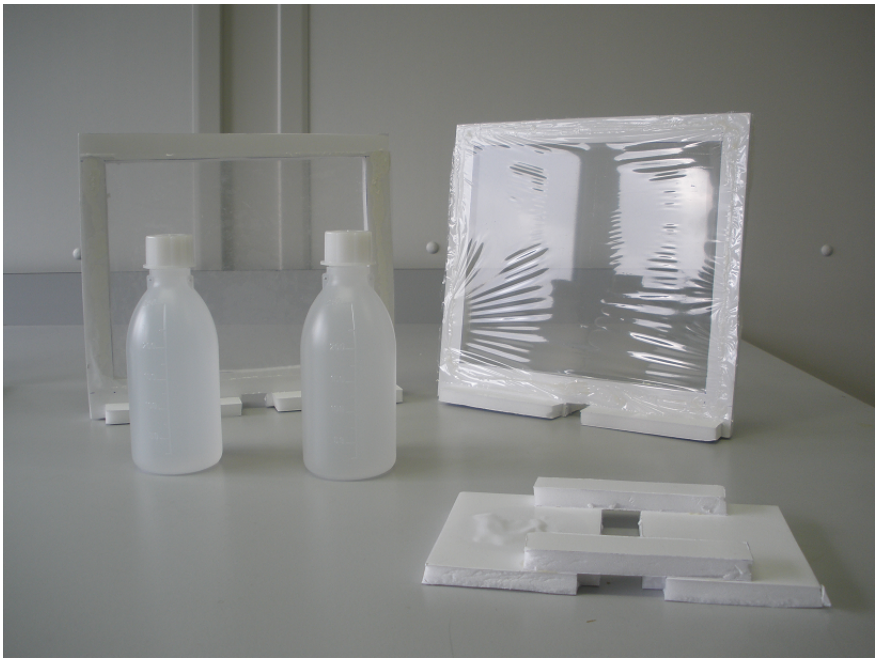

Figure 3.3: IR transparent windows frames, object support and test object (PE bottles).

Figure 3.3 shows IR transparent windows that act as frames where materials will be placed. The dimensions of the window frames are 30x25cm; the windows supports which keep firm a window have a hole in the middle-bottom to enable the placement of each window in the guide. Also in Figure 3.3, test object that are placed above the object support that is moved along the guide like the windows in the experiments.
Next step, it is plugged into a laptop, where IRBIS 3 Professional from Infratec is running and shows the IR image captured by the camera, the utilities of this program are explained in the next section.
After preparation of all equipment, such as test objects and window or windows at specific measurement points, IR camera connected to laptop and software ready, ten seconds are recorded for each measurement.
The experiments consist of: IR transparent windows, test objects or combination of them perform a gradual distance increment of 5cm step each ten seconds measurement. Each experiment requests a different kind of distance-step from the IR-windows and the test objects respectively. However, the IR camera lens in 0 cm from guide-ruler is the measurement reference system.

In each IR thermography record, the registration of each thermal record in the specific measurement will performed, and extracts relevant temperature information. The process to obtain the information begins by marking the relevant part of the IR image with a rectangle. Spatial average extracted for each recorded frame is saved in a table. The information is inserted in Excel table where a temporal average is calculated. The results obtained are temperatures measured for each distance. The reason for making two averages, spatial and temporal, is to decrease noise effects.
All temperatures measured for each distance is attached in a new table to every temperature from each test. In every distance two temperatures are extracted, with and without windows. And those are used to calculate transmittance for each point:

$$Transmittance = \left(\frac{T_{With}}{T_{Without}} \right)^2 \tag{3.1}$$

After all transmittances are calculated and inserted in each test table, transmittances are plotted on different graphs from where relevant conclusions are extracted.

3.2. IRBIS 3 Professional

IRBIS 3 Professional is the program used to control IR camera by laptop. This section is a brief introduction of the important parts of this program. See below, Figure 3.4 the GUI of the acquisition mode:

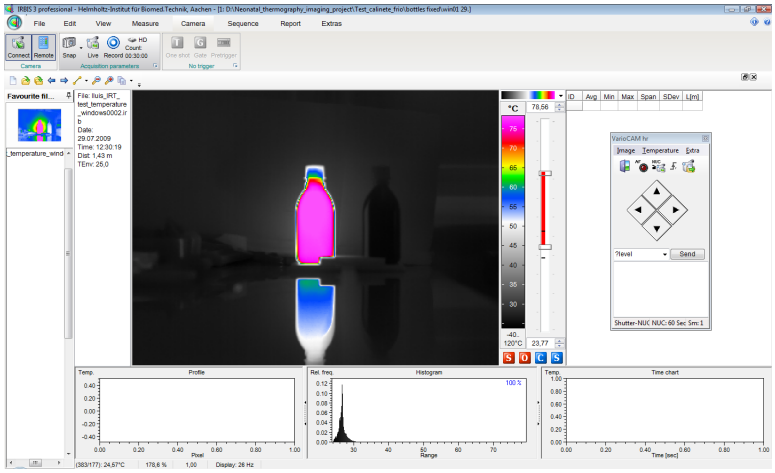

Figure 3.4: Graphical user interface (GUI) of IRBIS 3 Professional.

Focusing on the menu bar, at top of GUI (Figure 3.4), there are different menus such

as File, Edit, Measure, Camera, Sequence, Report and Extras.
First, File menu (Figure 3.5) has typical options as is seen in following:

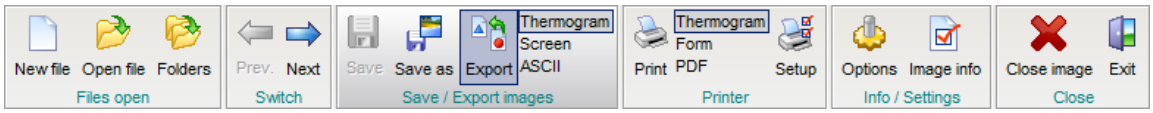

Figure 3.5: IRBIS File menu.

The typical options in this menu are New File, Open File, Folder that permits opening all IRBIS files in one folder, very useful for sequences, Save-Export image to save the infrared image in different formats: IRBIS file, Thermogram, Screen or ASCII; Printer, Info/Setting and Close. Edit and View menu are not necessary to do all functions needed in this experiment.

Figure 3.6: IRBIS Measure menu.

Measure menu, Figure 3.6, has two main important options, Measure areas and Correct areas. Measure areas are a kind of shapes that the user can choose to extract temperature information as average, maximum and minimum. The correction area is an option, that through different shapes it is possible to correct different kinds of schemes; one of these is object through window as is shown in the next figure:

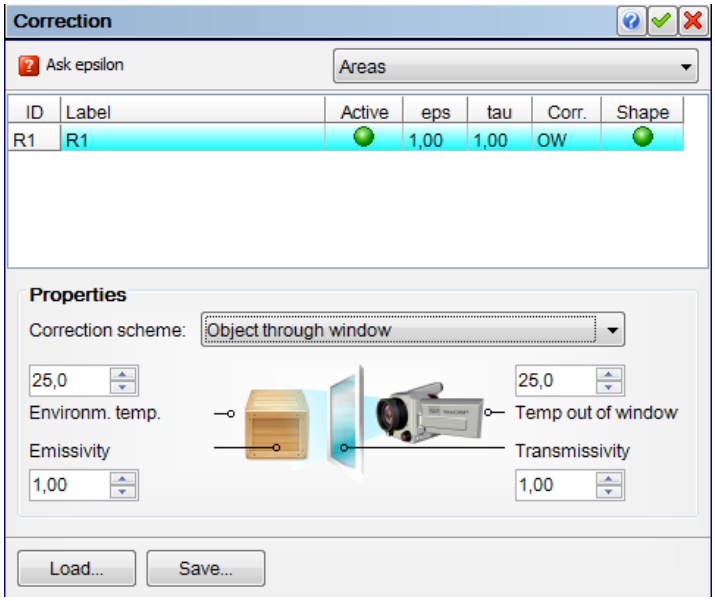

Figure 3.7: Correction options.

Figure 3.7 has two different parts. The top part consists of all correction areas and the bottom part the properties of each correct area. In this case, the single area corrects Object through window. Object through window has four parameters that the user can modify to adapt a concrete area to real temperature. Temp out of window is environment temperature outside the window, Environm. Temp. is environment temperature readout inside the window, Emissivity is the defined emissivity in chapter two and Transmissivity is an obsolete word that now is Transmittance and this term is also widely explained in chapter two.

Figure 3.8: IRBIS Sequence menu.

Next menu is Sequence menu (Figure 3.8) that has two important options, Play and T. diag. Play is the control of the sequence to view it like a movie. T. diag. shows temperature graphs on a specified area selected with Measure areas. In this graph the average, the maximum and the minimum of the selected area appear. Its data can be saved in plots or in a table with the complete data, the last one results to be really useful for this experiment to export the temperature data to excel tables.

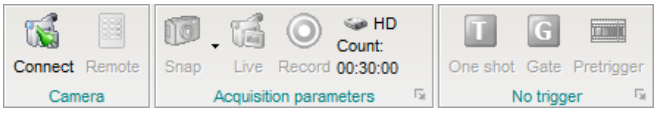

Figure 3.9: IRBIS Camera menu without connection.

One important menu in the IRBIS 3 Professional is Camera menu, Figure 3.9. Camera menu is really important because it has all the options to connect the camera to a laptop.

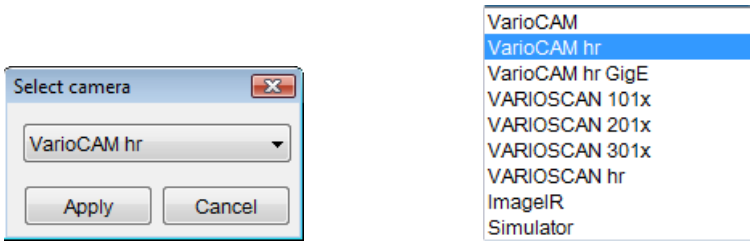

Figure 3.10: (a) Select camera window; (b)Kind of cameras to connect.

To realize a connection, first at all, the user has to click to connect icon. After click, a selected camera window (Figure 3.10a) has appeared, the user then chooses the camera that will be connected as seen in Figure 3.11b.

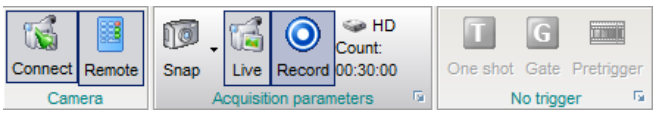

Figure 3.11: Camera menu with connected camera.

After Apply, choose correct camera, in the camera menu new options are activated, Figure 3.11 represents the remote and acquisition parameters. Acquisition parameters are Snap, Live, Record and Record options. Snap takes one single image from camera. Live shows live IR-images from camera like an ordinary camera. Record starts to record the captured image from camera with specified parameters adjusted before in Record options. Record options are the parameters to record IR-sequences, as viewed in Figure 3.12.

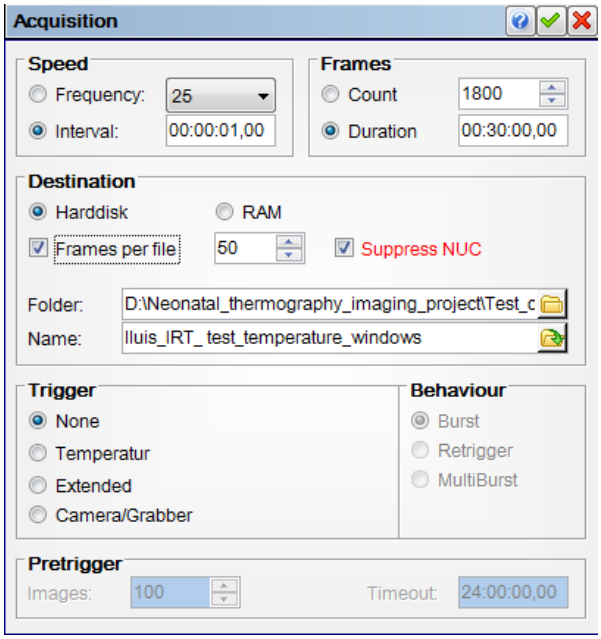

Figure 3.12: Acquisition options.

Figure 3.12 has three important options that are speed, frames and camera-object distance. In Speed, user can choose Frequency or Interval of time between frames. The thermography frames have a count-parameter; which is the number of frames in the sequence or Duration is the sequence time. In Destination, the user has two options to save the sequence, Hard disk or RAM. RAM should never been chosen because this means that the sequence is saved in RAM and it can saturated RAM, in consequence some part of the sequences could be lost. Saving the sequence in hard disk is necessary to determine some options, Frames per file is number of frames in each file. Folder is the folder where the sequence will be saved. Name is the name of those files.

Furthermore when Remote is clicked, a virtual remote control of the IR camera appears. This virtual remote control has different options that the IR camera can execute. The most significant are autofocus (AF) which focus automatically an object in FOV, camera's temperature shows the internal temperature of the camera while it is working and object distance gives you the estimated distance of focused object by camera, but is not really reliable.

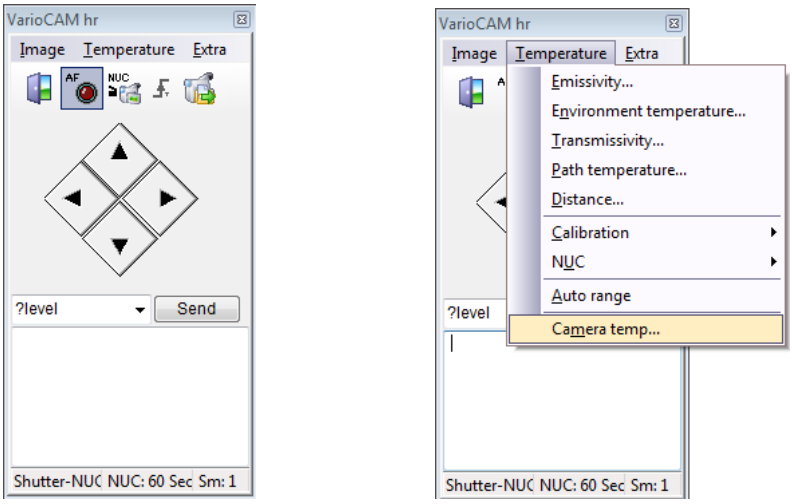

Figure 3.13: (a)Virtual remote control; (b)Temperature options in remote.

Figure 3.13a is the virtual remote where the AF is marked and in Figure 3.13b it is the Temperature menu which contains Distance and Camera temp.

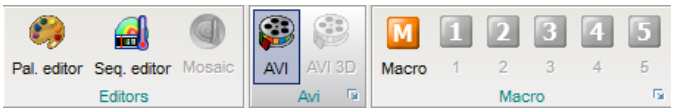

Figure 3.14: Extras menu.

The last menu is Extras menu, Figure 3.14, that the only option useful for the project is AVI which transforms a sequence of IR file to an avi movie.

3.3. Infrared (IR) thermography calibration tests setup

3.3.1. Room temperature object

The first group of experiments is the measurement of the effect that each window has throughout the meter with a test object at room temperature.

3.3.1.1 IR transparent window PEF 0.1mm

The following diagram represents the PEF transmittance 0,1mm along a meter on a test object at room temperature and also the graph of background image:

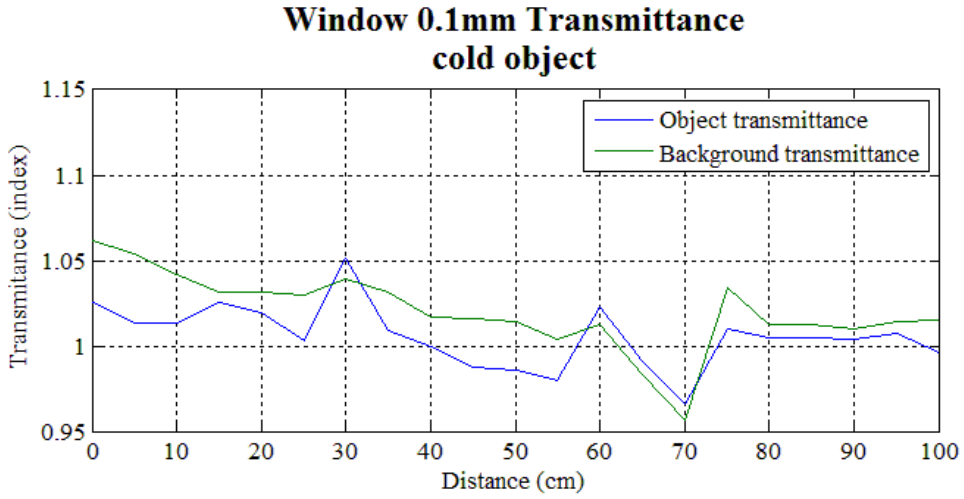

Figure 3.15: Window 0.1mm Transmittance; Test object versus Background.

In figure 3.15 it is remarkable that all values are over 1, excepting the transmittance at 70cm. In the background graph it is observed that the behavior is the same in both measurement zones. This means that it is not a measurement error; on the other hand, it does mean that both temperatures are not taken from the object at the same time, with and without windows. For that reason the temperature taken at 70cm may not be taken as good result in this measurement. In spite of that, it is possible to notice that the graph contains certain information that will be discussed later with both windows graphs.

3.3.1.2 IR transparent window PEF 0.5mm

The next case is analogous to the previous one, but with different material, the PEF 0.5mm. It is possible to follow the transmittance of the object at room temperature as seen below:

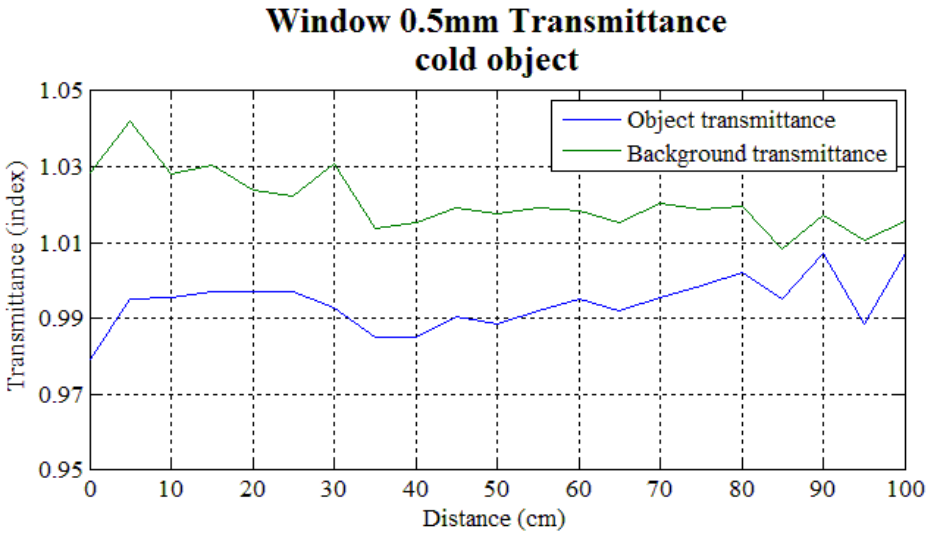

Figure 3.16: Window 0.5mm Transmittance; Test object versus Background.

In figure 3.16 the transmittance behavior is similar to the figure 3.15 transmittance because obtained results are bigger and closer to unity value.

At first sight, it is surprising that both graphs do not fulfill the electromagnetism theory which explains that all electromagnetic waves, on changing the means of transport, divided the signal in two, reflection and transmission, and the divided factor depends on the material. As Infrared is a kind of electromagnetic wave, it is impossible that the transmittance will be bigger than 1 in any case, even though the material is transparent it has always a part of the wave reflected.

The mistake is that all the influential parts in environment out the system have not been considered. For that reason it is necessary to review all the matters in the measurements that the transmittance has produced which will be bigger than 1. First, it is taken a look to the rest environment without considered system. There is no heat focus apart from the room temperature that could influence in this problem. One option is that the test object at room temperature stays at 5cm from the hot test object and hot test object warms up cold one. If that was the case, it always happens, with and without windows, and it does not disturb the results. In the end, the only element that generates heat and emits directly to the window is the infrared camera. Now, the camera is also considered as a heat source; and for that reason at the moment of the impact of the IR thermography signal on the window the signal is divided in two, the transmitted and the reflected signal. In spite of the fact that the window reflects low energy of the camera signal, this signal is bigger than the one transmitted by the object at room temperature. The signal recorded through a window is the sum of the transmitted signal from the test object and the signal reflected from the

camera by window. Furthermore, observing the reflexivity of the camera in both graphs, if the camera is close to the window transmittance is bigger, this fact strengthens the previous theory.

3.3.2. Hot temperature (85C to 68C)

The following experiments are carried out to verify the linear behavior of the windows at high temperatures. For this reason, the temperature is taken close to boiling point. The water is boiled by electric heater. The recorded temperature from the test object filled with hot water is approximately 85C. The object cools down owing to the impossibility to maintain a constants hot temperature. Consequently, the interval to take the temperature will be between 70C to 85C. In few measurements the test object temperature arrives to 68C because it is preferable to take all the measurements and finish all de distance for each position than break the measurement and reheat the water.

3.3.2.1 IR transparent window PEF 0.1mm

Next graph represents the transmittance of PEF 0.1mm:

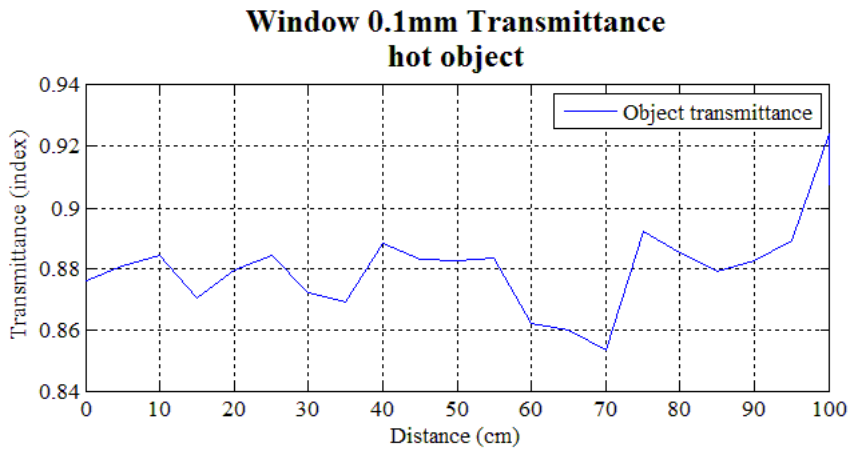

Figure 3.17: Window 0.1mm; hot test object transmittance.

Figure 3.17 follows a tendency of transmittance of 0.88 that stays of sorts constant until 60cm and till the 70cm transmittance has a small deviation of 0.86, then returns to the 0.8 and finally at 100cm goes to 0.92.

3.3.2.2 IR transparent window PEF 0.5mm

Next graph represents the transmittance of PEF 0.5mm:
In figure 3.18, the transmittance-value is very linear until 75cm and the value is 0.79. After

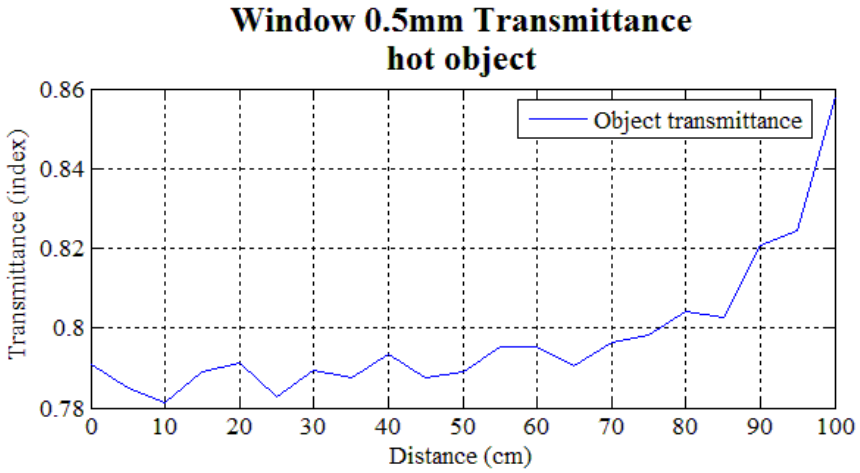

Figure 3.18: Window 0.5mm; hot test object transmittance.

75cm the transmittance grows linearly until 0.86.
Both previous graphs are most interesting because it is the direct comparison between both windows on a same object at hot temperatures. The first observation is that the PEF 0.1mm has a better transmittance; this gives a more exactly calibrated result without carrying out an elevated compensated temperature. On the other hand, the PEF 0.5mm is most stable; it means that the fluctuation between the results is small, that has to be taken in to account because in small variations this material looks less affected than the PEF 0.1mm. All of these considerations; must be taken carefully because they are taken under bad condition. The worst is that the measurements with and without IR transparent window are not made at the same time and it changes the conditions, besides the test object temperature cool down.

3.3.2.3 IR transparent window PEF 0.1mm versus PEF 0.5mm

In this case; it shows that how the measurement is affected by putting both windows at the same time and different distances. Also it verifies the effect to put one or other window in front of the camera. For that reason the graph result has 3 dimensions: at plane XY is the distances of the window of 0.5mm and the 0.1mm and in axis z is the transmittance.

In figure 3.19 it is noticed that the transmittance of the trace stays over 0.7 for all the

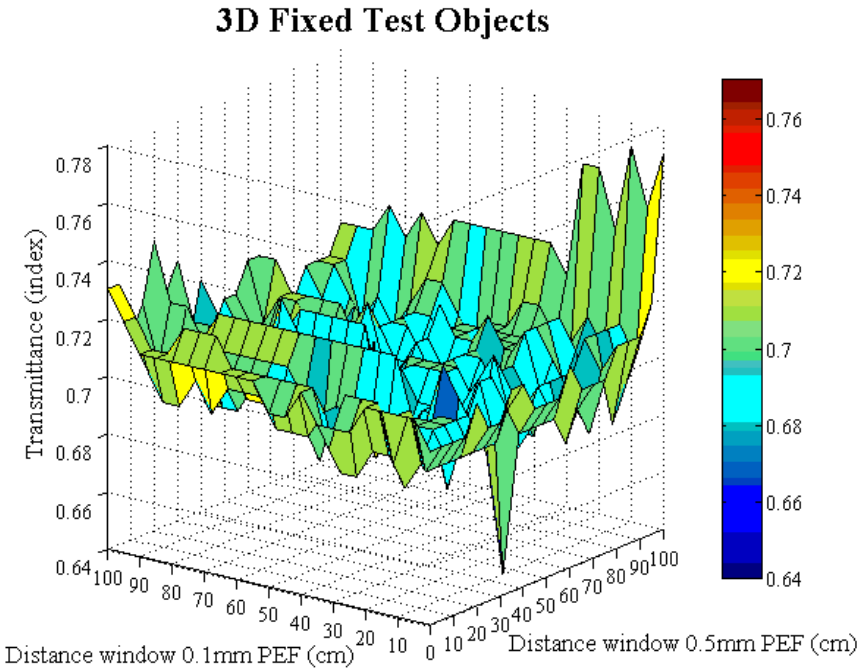

Figure 3.19: Two windows transmittance 3D.

distances except few cases. It is extracted two conclusions. First, the behavior of both windows between the camera and the object has the same behavior as one alone, but the transmittance decreases as expected. Second, it never minds which of both materials is in front of the camera, the behavior is always the same. This means that the behavior of the window's transmittance is lineal along 1 meter. These variations are induced by the bad conditions of the environment that the measurements are carried out, i.e., no constant environment temperature, with and without windows measurements uncorrelated in time and cooled down test object.

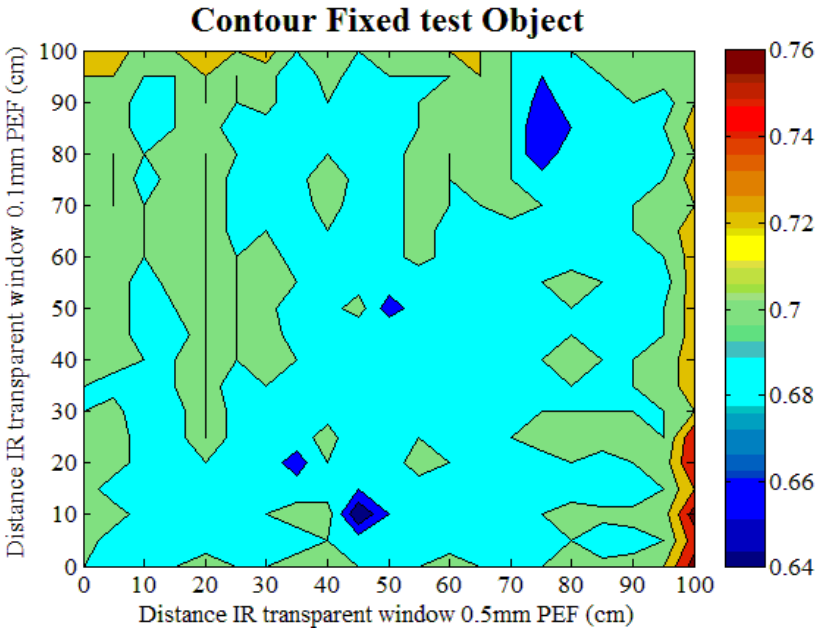

Figure 3.20: two windows IR- transmittance contour.

In figure 3.20, which is the representation of that most transmittances are between 0.68 and 0.70; this strengthens the previous IR transmittance theory.

3.3.3. IR transparent windows versus test objects

Both followings measurements represent how affects the transmittance at the distance between the camera and window and, most important, the distance between the window and test objects. Due it has not sense to put the test object in front of the windows because the transmittance is 1. In graphs appears with a constants value in order to it is easier observe the most relevant dates that is that the test objects are behind the window.
The measurements carried out to the test object will be at 10cm from the window because the initial design does not consider this kind of measurement. Furthermore, the closer measure from the test object to the camera is 20cm that is much closer the test object could occupy all field of view (FOV) and then the reference could be lost and the result becomes irrelevant.

3.3.3.1 IR transparent window PEF 0.1mm versus test objects

In this first case, it is compared IR thermography window of 0.1mm distance to test object distance. In figure 3.7 and 3.8 the value of direct vision to test object is 0.8 to see the results better.

In the Figure 3.21 the transmittance is approximately 0.87, same as it was obtained when

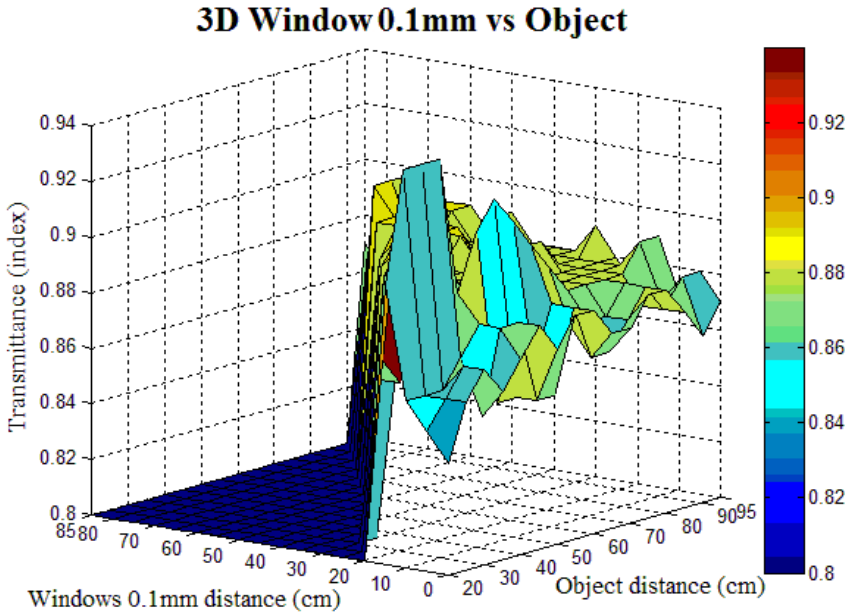

Figure 3.21: Window 0.1mm versus Test object 3D.

the test object was fixed at the 100cm. This means that the transmittance in window of 0.1mm is constant along a meter independently of the distance between IR camera and the distance between test object.

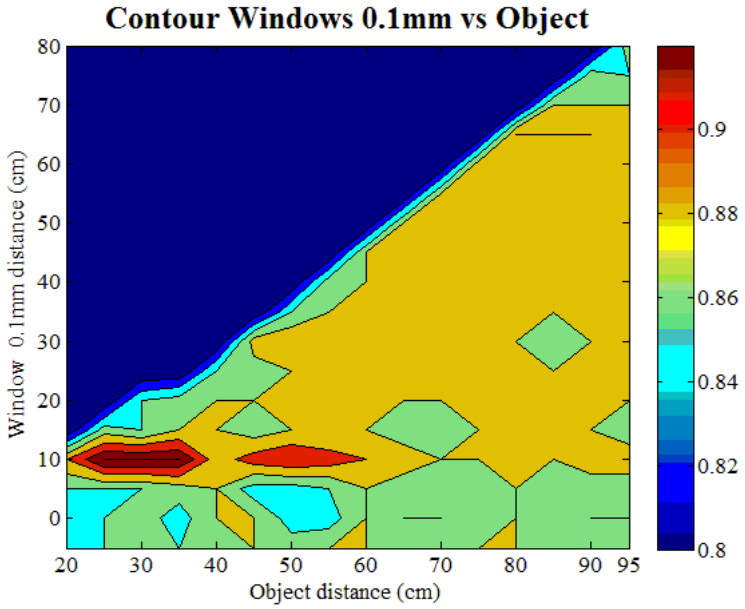

Figure 3.22: Window 0.1mm versus test object contour.

Figure 3.22 is useful to clarify the results extracted with figure 3.21. In the figure 3.22, it is recognizable that; in the measurements of window 0.1mm at 10 cm distance, it has a higher value than other, this is because the mentioned bad-experimental conditions to carry out the measurements.

3.3.3.2 IR transparent window PEF 0.5mm versus test objects

In this other case, it is analogous to previous case, although used window is 0.5mm width. In figure 3.22 and 3.23 the value of direct vision to test object is 0.69 to see the results better.
In figure 3.23 and 3.24 respectively; it is able to see how the transmittance at the window of 0.5mm is in this case 0.78 with more fluctuation than the last case. In that window the transmittances with the test object at 100cm or with the test object changing position are more similar than other case.
Then, the conclusion is that in a meter of measures the behavior of the windows over the hot object does not matter the distance of the window and the test object because the transmittance does not have a perceivable variation in any case.

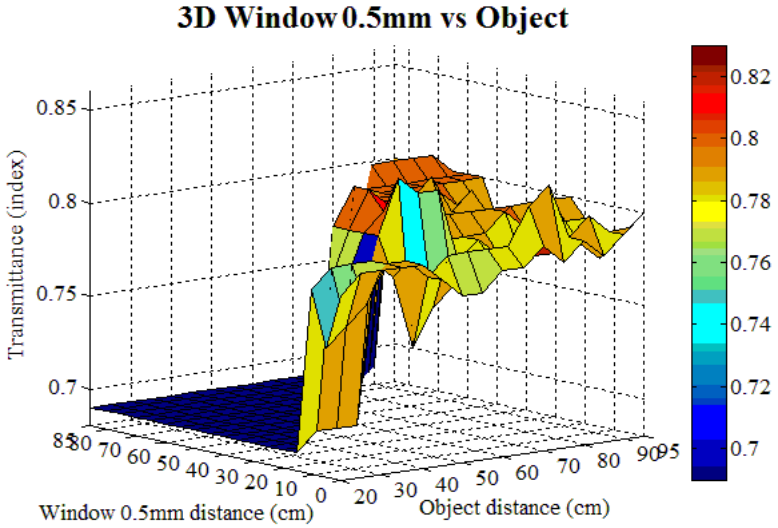

Figure 3.23: IR transparent window 0.5mm versus test object 3D.

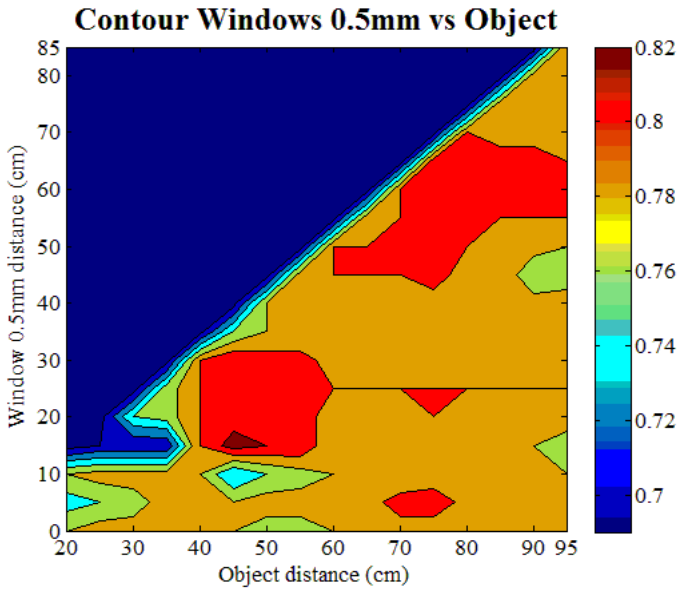

Figure 3.24: Window 0.5mm versus test object contour.

3.3.4. Hot to environment temperature

Another interested experiment consists in measuring directly whether the transmittance changes for temperature variations. In order to do that will put one of the windows in a middle distance but just cobbering one test object. Then, water is warmed up; the two test objects are filled, and the record is begun.

3.3.4.1 Continuous measurement

The next graphs measure the temperature in a large time period, the time necessary to cooling the water inside the test objects until a room temperature.
In this first intent, measurement of the transmittance at different temperatures is recorded three and a half continued hours, there engraves one frame for each second, because the temperature variation less than one second is insignificant.

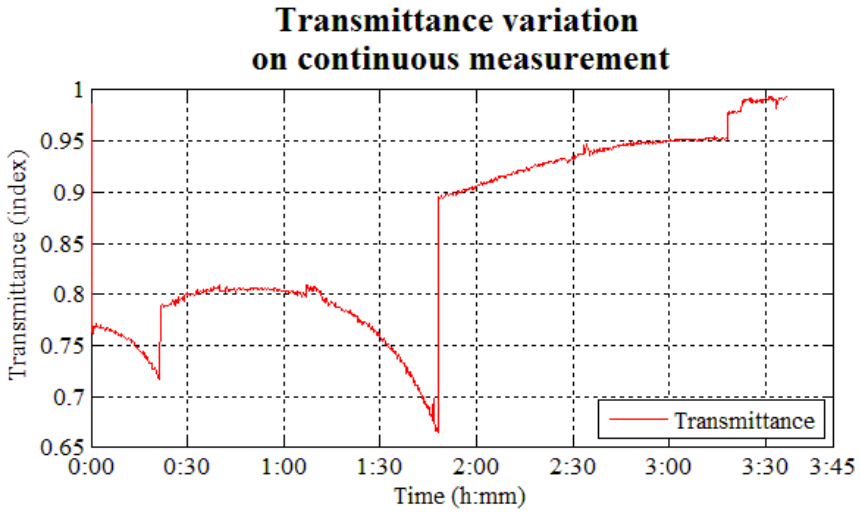

Figure 3.25: Transmittance variations on continuous measurement.

Figure 3.25 and 3.26 shows results totally unexpected. Because the test objects temperatures are making unreal jumps of temperatures, it is impossible that test objects warmed themselves, at same time and in several times.
It happens visibly for camera blame. The most reasonable explanation for these jumps temperatures is the intermittent recording made by the camera at certain time where an autofocus and a readjust the image resolution are realized. This explains the jumps which are a problem or a limitation of the camera that is not able to follow high temperature variations

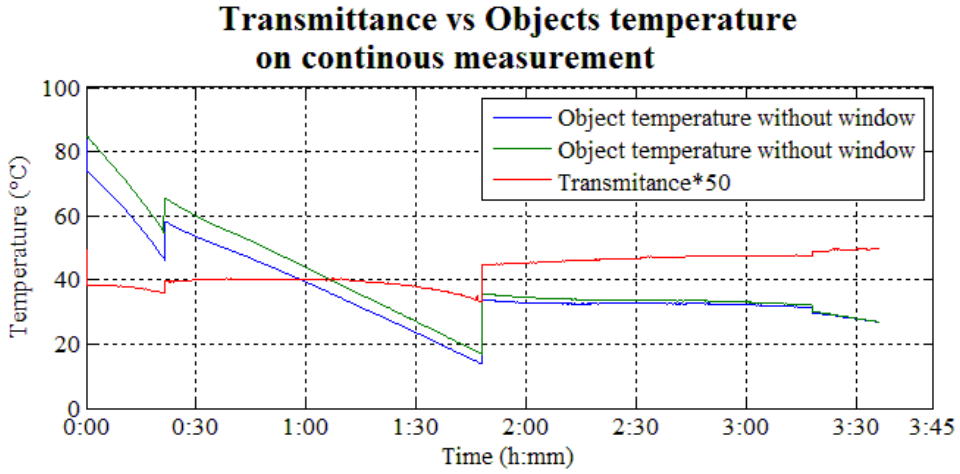

Figure 3.26: Test objects temperature on continuous measurement.

in a long time period. In spite of that, this limitation does not produce any misfortune in this project because the temperature variation will be 5C in this project. It is because the incubators are under temperature control.

3.3.4.2. Intervals of 30 minutes measurement

In order to trying to solve the limitation of the case before new experiment is proposed to change the continuous record to intervals of 30 minutes with the same duration. As seen below:

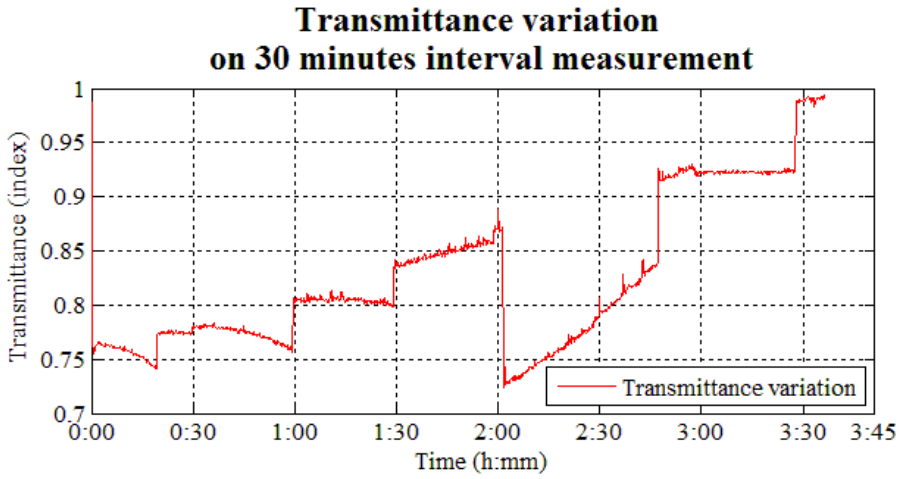

Figure 3.27: Transmittance variation on intervals of 30 minutes measurement.

It is possible to verify that the transmittance graph and the temperatures graph have the same problem as previous one, but these are worse because these have more jumps. These jumps are caused for the interrupted record as seen in figure 3.27 and 3.28 where each 30 minutes have one of these jumps.

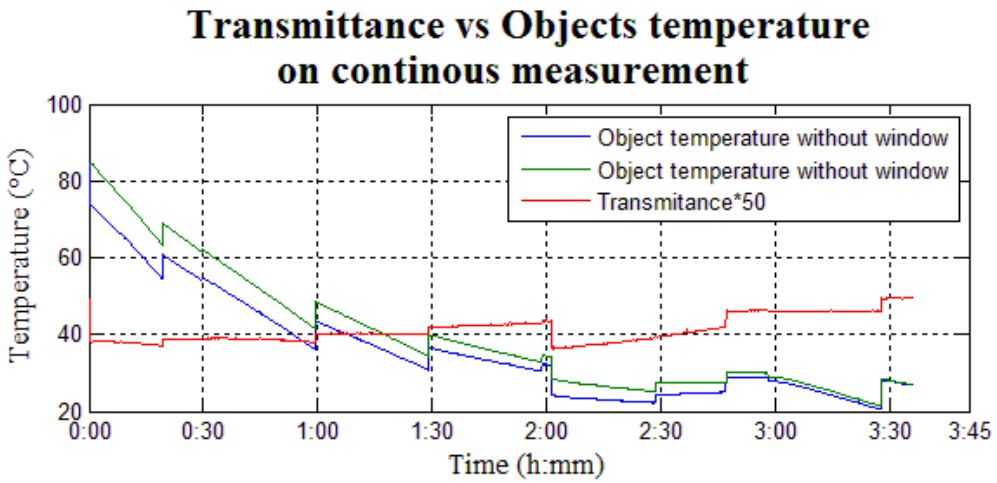

Figure 3.28: Test objects temperature on intervals of 30 minutes measurement.

3.3.5. Camera versus Environment temperature

One important fact for calibration is to know camera temperature during the experiment. Here it is compared camera and environment temperature during the measurement of transmittance of the PEF 0.5mm.

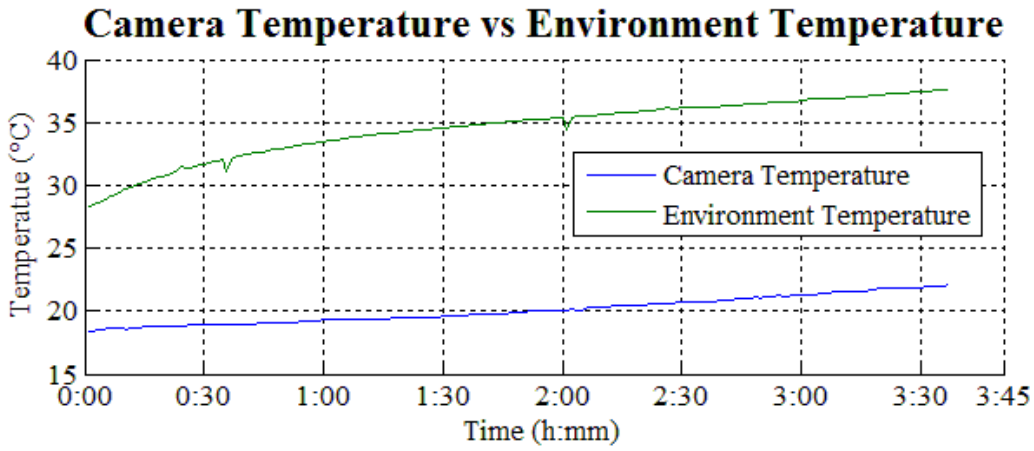

Figure 3.29: Camera versus environment temperatures.

Figure 3.29 shows the variation of internal camera temperature compared to environment temperature. The environment temperature variation is produced by day light, i.e., the measurement is taken during a morning. It starts at 10:00 a.m. when the sun start to warm up the room and the measurement finishes at 1:35 p.m. when the sun warms up more the room. IR camera temperature behavior warms up hardly the first hour and the rest hours the temperature increment is linear like environment temperature. First hour the IR camera is stabilizing and the others hours it is increasing analogously to the environment temperature.

3.4. IR Transmittance values

Besides, it has more IR transparent materials in a different spectral bandwidth. In the next table presents few measuring objects and the spectral bandwidth that each object is transparent.

In the Table 3.1, Polyethylene (PE), tested material, is the material that has more spectral

Measuring object	Spectral bandwidth $\Delta\lambda$
Glass	4.8 ... 5.5μm
Polyethylene PE	3.4;(6.8);13.8μm
Nylon	3.0;3.4μm
Flame	4.4μm
Iemperung Si-layer	3.6 ... 4.4μm
PUR-Lack	4.4;(5.8);(6.5);8.0μm

Table 3.1: Spectral bandwidth.

bandwidth, i.e. PE is most versatile material to use in this project because it can use with every kind of IR cameras.

3.5. Discussions

As first experiments is showed that is not recommended to work with material in room temperature, because the camera's heat reflection to the window affects a lot in the measurement and unreal results are given. A possible solution for this reflection would be to incline the window 45° and in that way all reflected waves goes to another direction. In the direct comparison carried out between both materials it has obtained two results and it is necessary to choose which one is the best for that case. On the one hand, the PEF 0.1mm has a higher transmittance is which looks for, on the other hand the PEF 0.5mm is the more stable in them measurements and that is what is looked in all measurements. At least PEF 0.5mm could be the chosen one as a window. But it allows for that this decision is taken with the foregoing bad conditions. In that case it is not necessary to use two windows but gives more information that could be useful in the future for possible applications Furthermore in one meter variations the window's properties are lineal and this is favorable for any application, normally. In spite that, the distance changes between window and test object, the behavior of window stays lineal. This allows putting the test-object at the best distance. The most surprising result from all the experiments is the bad behavior that camera has doing a long record where the temperature goes down. In spite of that, it is not relevant in this case, because the temperature variations in the incubators will be **35C to 40C**.

4. Infrared image processing

In this chapter; the image processing of the infrared thermography will be presented. The core of the infrared thermography image processing is a design of virtual temperature sensor, which used for tracking region of interest (ROI) of the subject undergo medical thermography. The concept of virtual sensing system is based on the active tracking of specific object characteristics such as, surface area, contouring shape, intensity, angle and other anatomical properties. The algorithm implemented in this project is basically consisting of five stages which are: Infrared (IR) video acquisition, geometry (shape) selection, shape coordinate setting, ROI template matching and finally tracking ROI template throughout the image plane.
The developed image processing function in the virtual sensor concept is to extract the information from an acquired thermal video. The implemented function of the tracking method works as a virtual temperature sensor. For this point, we consider the IMAQ vision toolkit is a powerful library of image processing functions in the LabVIEW platform, is used. In this chapter, the developed virtual sensor concept could be applied in different clinical procedures in the neonatal intensive care unit (NICU); to trace the surface temperature of the newborn. Furthermore, the image processing step is used to solve the tracking problem of facial and other anatomical structures which are subtle to long-term clinical mentoring approach. The core of this application is to capture infrared thermography frames from the IR camera and follow a region of interest (ROI) along the acquired frames. This ROI is selected by the user manually, after ROI selection the algorithm tracks this ROI on the specified frame. After that the ROI reference coordinate is defined and extracted from the rest of the active thermogram (image), then the quantification of the intensity value in the thermography frame is performed to quantify and converse the actual temperature value. All image processing steps were implemented in real time fashion. The tracking process can be divided into five principal stages, which are infrared acquisition, ROI geometry and coordinate definition, tracking coordinate matching for the object, ROI temperature level extractions and finally temperature trace display.

4.1. Tracking software implementation

As the tracking software divided into five main stages as previously described, figure 4.1 illustrate the signal flow diagram of the tracking algorithm with its related signal notation and level.

The block diagram illustrated in figure 4.1 present the main steps in the tracking algorithm

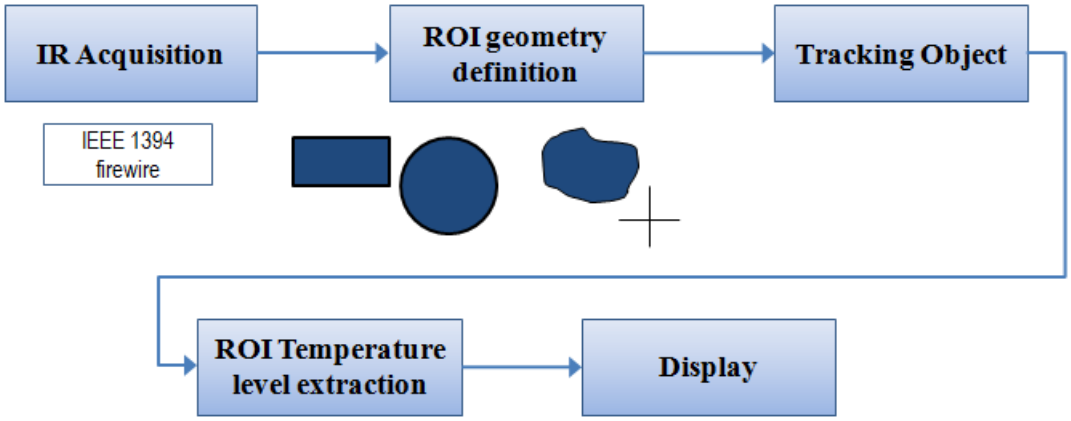

Figure 4.1: Image processing block diagram.

as follows. IR-Acquisition block transforms the infrared (IR) data frame from manufacturer define format (IRB) of the thermal camera to an appropriate video format (e.g. avi) using video coding algorithm. The second step in the algorithm is ROI geometry and reference coordinate definition by which the region of interest (ROI) sub- image can be defined and the active coordinate of the selected ROI is set for tracking process.
The third stage in the block diagram is the Tracking object step, the main function os this block is to follow and the trace the selected ROI throughout the thermography frames. The ROI Temperature level extraction block, is responsible for extraction and isolating the ROI coordinate from the rest of the image. Furthermore, the temperature level data is extracted and identified. Finally, the last block, Display, presents the acquired IR image with overlaid ROI and displays the temperature information extracted from ROI.

4.2. Infrared thermography acquisition

The measurement setting of the infrared thermography image acquisition and processing is illustrated in figure 4.2, the infrared thermography imager detect the thermal radiation energy of the subject with the temperature (Tobject) against relatively colder background with the temperature (Tbg). The acquired infrared thermography data transferred to the measurement laptop through IEEE-1394 (firewire interface) with speed of 25-50 frames per second (fps). The IR camera used in the experiment is long wave infrared energy (LWIR) detector VarioCAM hr head (from Infratec GmbH, Dresden, Germany). The infrared (IR) detector technology is based on the un-cooled embedded focal plane array (FPA) detection

module. The temperature resolution for noise equivalent temperature difference (NETD) of IR-thermal camera is about (0.05C) at 30C operating environmental temperature. The spectral band width of the IR camera lies between 7m to 14m. The infrared image acquisition and preprocessing was perform by IRBIS thermography processing platform which is the driving software for the infrared thermography camera, by which the video conversion and temperature drift compensation, camera calibration and histogram equalization takes a place before main tracking algorithm application.

The infrared thermal acquisition library (IRBIS SDK-platform); is not efficient to acquire

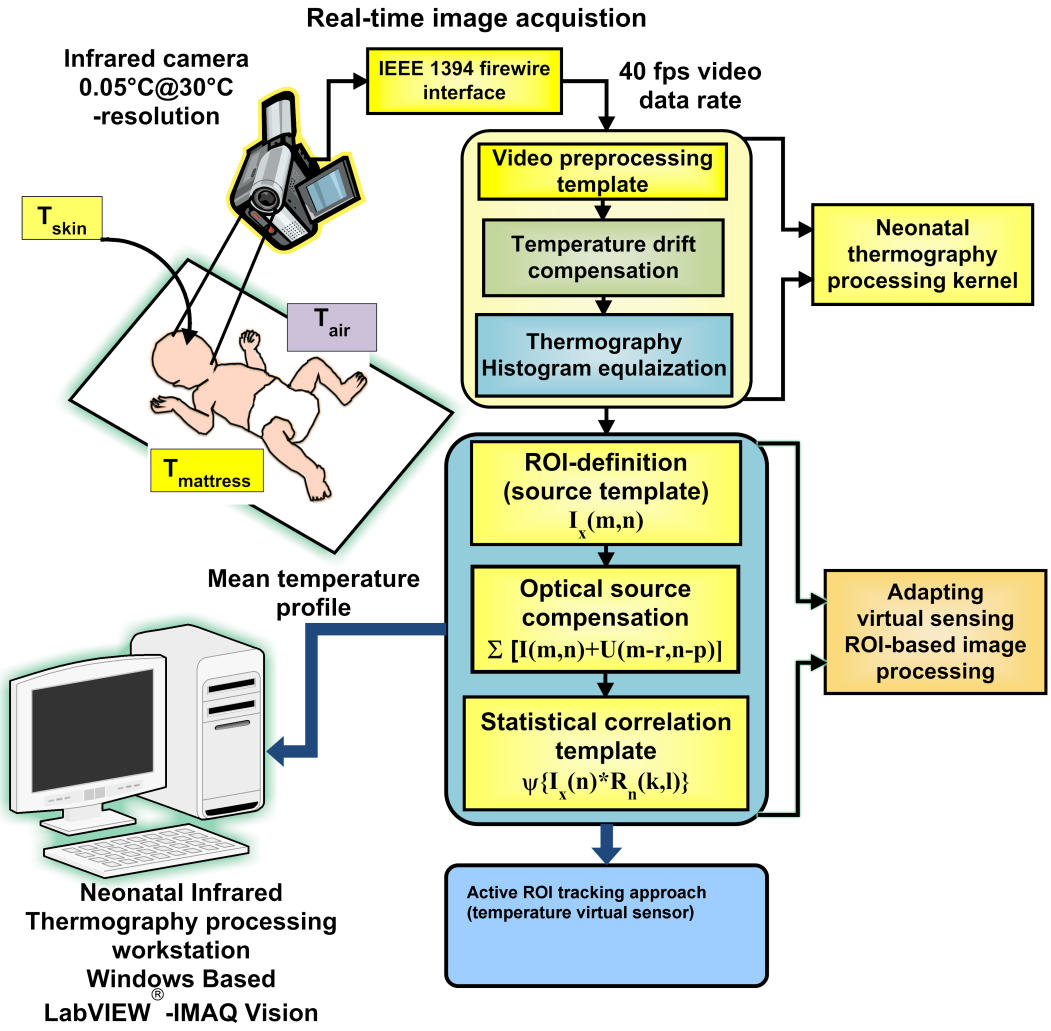

Figure 4.2: The block diagram of the infrared thermography setting used in the ROI tracking system.

the real time thermal data due to the lack of the proper IEEE-1394 firewire functionality, to be interface the thermal data form the IR thermal camera to the LabVIEW platform. The alternative to that process is to use thermal video data converted from acquired thermal

frames.

4.3. Tracking methodolgy

The goal of this project is to develop a specific tracking methodology that can accurately monitor the motion of the incubator newborn. The method goes through four steps to track specific object. First step, the user draws a shape in the region of interest (ROI). This ROI shape will be the tracking object. The second step is the coordinate (shape) matching where it is found the coordinate of the template in new frame. The third step is to replace the ROI from the old coordinate to the new coordinate. Finally, the extraction of ROI intensity information is made. The matched ROI is isolated from the rest of the image and is extracted the color intensity value.

Figure 4.3 presents the flow diagram of the tracking methodology. Two first steps, IR

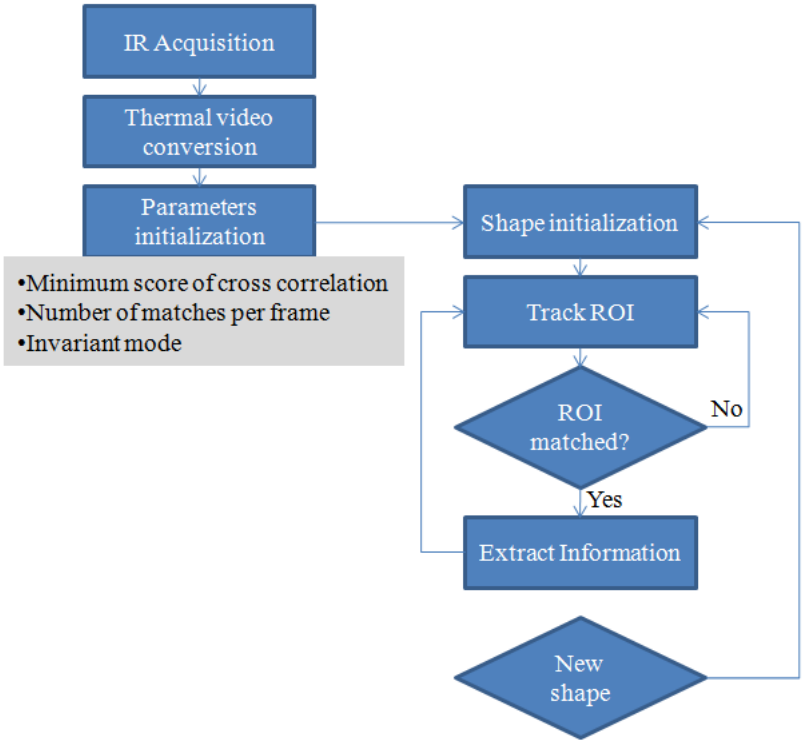

Figure 4.3: Flow diagram of the tracking operation.

acquisition and thermal video conversion are explained in previous section. Parameters initialization has three parameters that the user must define before the tracking starts. The minimum score of cross correlation is the minimum value that one cross correlation in matching process to accept it like a ROI matched. Number of matches per frame is a quantity of

matched ROI which will be found per frame. Invariant mode has two modes to search the template ROI: shift invariant and rotation invariant. The shift invariant mode does not allow rotation of potential matches in relation to the template, i.e. only matches with the same orientation as the template are found. The rotation invariant mode allows in any direction in the camera plane; this mode is significantly slower than the shift invariant mode, because template profile is shifted by amount of rotation.
The shape initialization is the drawn shape by the user. This shape will be the matched ROI in the thermal video. Track ROI is the part that is found the new coordinate of the ROI in successive frames. If in one frame the ROI is not matched, it should to track in the next frame. If the ROI is matched in the frame, next step is extract color information. The extract information carries out the ROI adaptation and the ROI intensity information. The ROI adaptation deletes the ROI in the old coordinate and places the ROI in the new coordinate. The ROI intensity information extracts the color information from the matched ROI. The new shape is an interruption made by the user to draw a new ROI shape and starts the process with the new ROI shape.
This manual step should be further improved in the later active tracking system in order to highlight the interested anatomical structure to be traced automatically and in intelligent approach.

4.3.1. ROI-shape definition

The first stage of the tracking thermography image processing is the selection of the region of interest (ROI) into the image. The ROI will be an arbitrary shape drawn by the user. The template ROI is used to match it in the new frame. For this reason, the global rectangle, the contour (shape) and center reference are required to the coordinate matching.
The global rectangle; is the minimum rectangle required to include the shape, its size is defined by [axb] and the coordinate origin is the top-left of the global rectangle. The contour is the drawn shape for the user and every shape points have their relative coordinate to the global rectangle. The center reference $(x_c, y_c)$is the coordinate of the center of ROI relatively to the global rectangle (see figure 4.4).

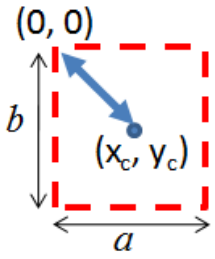

Figure 4.4: Definition of the center coordinate respect the global rectangle and the size of global rectangle.

4.3.2. ROI-coordinate (shape) matching

The matching process of the defined ROI coordinate was performed by applying a cross correlation operation between ROI defined template and the successive image frame as follows [Rel04].

$$C\left[i,j\right] = \sum_{x=0}^{a-1}\sum_{y=0}^{b-1} T\left[x,y\right] \cdot F\left[x+i, y+j\right] \tag{4.1}$$

Where $C[i,j]$ is the cross correlate matrix and i and j represent each point that is made the cross correlation. $T[x,y]$ is the matrix of the ROI defined template and $F[x,y]$ is the successive image frame.

In the figure 4.5 the yellow rectangles are some made cross correlation that are lower than

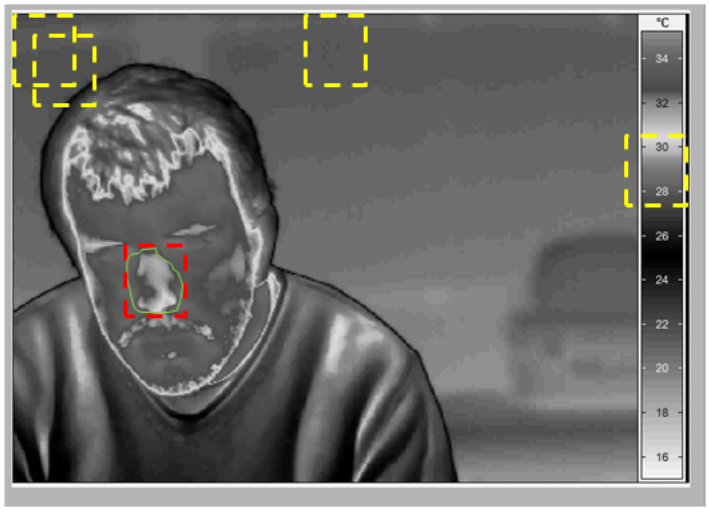

Figure 4.5: The cross correlation processing sample in the new frame.

threshold in the new frame and the red one is the matched rectangle that is higher than

threshold.
The chosen threshold was 70%. This threshold is chosen because it is the minimum optimal value which does not produce a spurious ROI matching. This threshold was chosen after the trial of the matching matrix with different threshold values, for the illustration of the thresholding-matching approach table 4.1 represents the selection truth table of the process.

Threshold value(%)	Frame with matching ROI	Frame without matching ROI
50	X	—
55	X	—
60	X	—
65	X	X
70	X	X
75	X	X
80	X	X
85	—	X
90	—	X
95	—	X
100	—	X

Table 4.1: Cross correlation threshold truth table.

The table 4.1 is a truth table that is compared the matching process with different thresholds in two different kind of frame. One frame contains a matching ROI and the other frame without matching ROI. The "X" in the column of the frame that contains a matching ROI represents the matched ROI with the threshold value in the same row. The "X" in the column of the frame without matching ROI represents the threshold value which does not find a spurious matched ROI template.
From the new ROI coordinate found, it is generated the new coordinate, (x_c^{t+1}, y_c^{t+1}) referenced from the center of the global rectangle and the new angle (θ^{t+1}) of matched ROI is used to adapt the ROI in new frame.

4.3.3. ROI-matching adaptation

The adaptation of the ROI to the new coordinate has three steps. First step is to change the new coordinate referenced to the center to global rectangle reference, as seen equation 4.2.

$$(x^{t+1}, y^{t+1}) = (x_c^{t+1} - x_c, y_c^{t+1} - y_c) \tag{4.2}$$

Where (x^{t+1}, y^{t+1}) is the new coordinate of the global rectangle frame.
Using the new reference; the ROI is placed (moved) to the new coordinate and the old ROI coordinate description is deleted, as illustrated in figure 4.6.

The figure 4.6 presents a sample of a replacing ROI from the old coordinate to the new

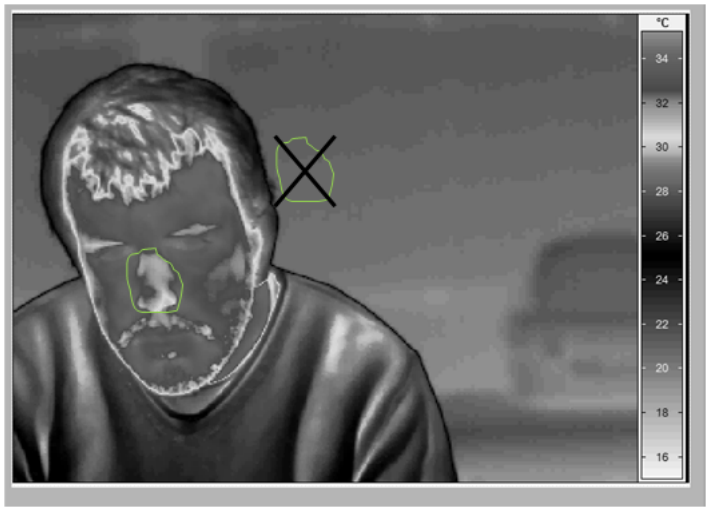

Figure 4.6: The new coordinate are placed and the old are deleted.

one. The labeled shape represents the old coordinate of the ROI and the other shape is the new coordinate of ROI setting.

4.3.4. ROI-intensity information extraction

Finally, the extraction of the intensity information from the matched ROI is made isolating the ROI from the rest of the frame and extracting the color level value.
In the process of ROI tracking-matching, the required (the active) ROI is extracted and the other image area is omitted, as equation 4.3.

$$ROI[i,j] = \begin{cases} F[i,j] & \text{if } x^{t+1} < i < x^{t+1} + a; y^{t+1} < j < y^{t+1} + b \\ \text{omitted} & \text{otherwise} \end{cases} \tag{4.3}$$

$ROI[i,j]$ is the isolated ROI. $F[i,j]$ is the image frame. The (x^{t+1}, y^{t+1}) array is the new (updated) coordinate with the a and b are the global rectangle size.

Figure 4.7 shows the result of the equation (4.4). This image is used to extract the color level information from the define ROI.

Figure 4.7: Isolated ROI from the global reference ROI frame.

$$ROI[i,j] = R_{ROI}[i,j] + G_{ROI}[i,j] + B_{ROI}[i,j] \tag{4.4}$$

The $ROI[i,j]$ is the isolated ROI sub-image matrix, $R_{ROI}[i,j], G_{ROI}[i,j]$and $B_{ROI}[i,j]$ are the primary color-space value in the isolated ROI region. The RGB color space is primarily divided into three components, red, green and blue. The division helps to quantify the color level easily.

The level color of the image is the average of each component color matrix.

$$\bar{r} = \frac{\sum_{i=0}^{a-1}\sum_{j=0}^{b-1} R_{ROI}[i,j]}{a \cdot b}; \bar{g} = \frac{\sum_{i=0}^{a-1}\sum_{j=0}^{b-1} G_{ROI}[i,j]}{a \cdot b}; \bar{b} = \frac{\sum_{i=0}^{a-1}\sum_{j=0}^{b-1} B_{ROI}[i,j]}{a \cdot b} \tag{4.5}$$

Where $\bar{r}$, $\bar{g}$ and $\bar{b}$ are the average of the level color in the image.

4.4. Subject-Camera plane representation

An important consideration in this project is the object rotation. All objects can rotate about three directions: axis x, axis y and axis z, as it is defined in figure 4.8. The rotation about axis z is solved thanks to the rotation invariant mode. The other two rotations have to be measured the rotation angle range and are considerate out-of-plane. The maximum angle rotation in the out-of-plane is shown in the table 4.2.

Figure 4.8 represents the schematic diagram of the facial rotation coordinates with the corresponding camera-system coordinates used in the tracking approach. The black square localized on the subject face; represents the projected image plane. The rotation about x-axis and y- axis is the out-of-plane which is limited by the tracking software implementation. Nevertheless, it is measured the angle range of ROI-plane rotation in the out-of-plane coordinate system. Furthermore, to approaching more accurate the measurement, this experiment is repeated with three parts of face: forehead, nose and mouth, in order to cover all the facial anatomical structures.

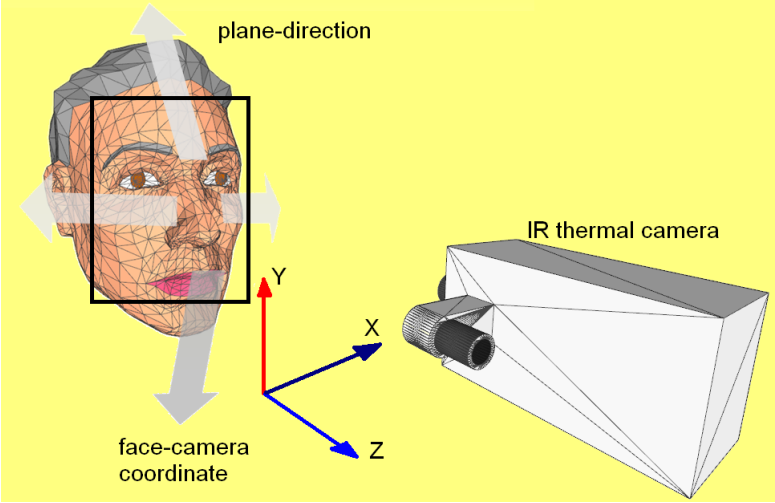

Figure 4.8: Out of plane facial rotation coordinate used in the active ROI tracking system.

Table 4.2 presents the angle range of the face. The rotation about axis x has the same

Face Part	Left rotation	Right rotation	Up rotation	Down rotation
Forehead	15°	15°	45°	30°
Nose	15°	15°	10°	25°
Mouth	15°	15°	30°	15°

Table 4.2: Angle range measurement.

angle range for each face part. On the other hand the rotation about axis y is really different for each face part. This is for the vertical symmetry of the face.

The main aim of implementation the ROI tracking method as a core of the virtual sensing technique, is monitoring continuously and in a real-time fashion, the temperature of neonate through out different clinical procedure, as Figure 4.9 illustrates the principal virtual temperature points to be observed and quantified continuously, with the aid of infrared thermography imaging method. The points mapping will be used for developing, an efficient and robust contactless and non-invasive temperature monitoring; and in advanced stages a neonatal-skin control mode.

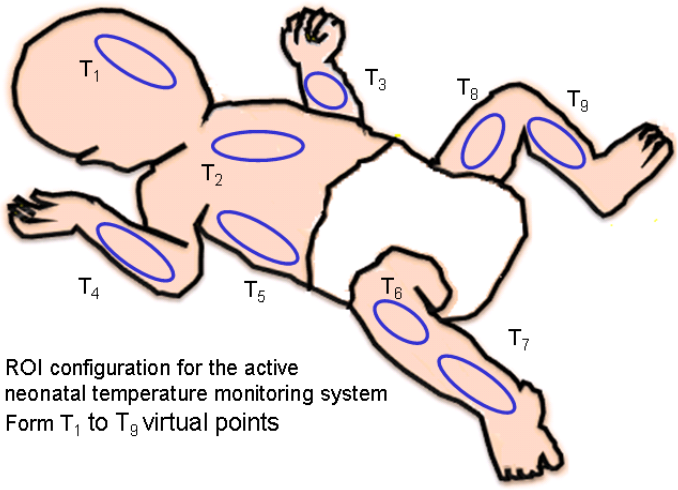

Figure 4.9: Clinical temperature point distribution on the neonate skin surface for continuous identification of thermoregulatory status of the neonate inside the neonatal intensive care unit (NICU) (reference, Obladen, 2003).

These multiple measurement point can be tracked in the proposed ROI tracking method by generating a selected template for these points as an ROI-based coordinates over the thermography frames acquired from thermal camera. After that, the temperature information from these points correspondingly [Bha76, Cho97, Cro75, Pom77].

5. Discussions and Conclusions

5.1. Discussion: Viability of IR-camera through incubator window

The incubator hoods are mostly made of plexiglas. The Plexiglas is an infrared reflective material throughout all infrared spectral radiation bands (SWIR, MWIR and LWIR) which is was known before the project began. Based on historical review, the infrared waves are also named calorific or calorie-thermal waveform, because this is the frequency band of the light range which contains the biggest part of light heat. As Plexiglas is reflective in infrared spectrum, consequently, the infrared energy radiated from neonate and the incubator itself, are reflected by plexiglas inside the incubator and the infrared waves keep inside. Therefore, the incubators are sufficiently effective in maintaining a constant temperature for the neonates.

On the other hand, as the infrared radiation is reflected by the Plexiglas, the thermal camera cannot receive any thermal information considering the interior structure of the neonatal incubator.

In order to overcome this problem, a small part of the incubator walls was replaced by suitable infrared transparent material, such as Polyethylene Foil (PEF) window. But in this case, a small portion of incubator radiative heat loss can be detected by thermal signature of the incubator hood. Consequently, the incubator must warm itself up constantly to maintain a constant temperature. The constant use of the heating system increases the system's power consumption. To summarize, if a frame of plexiglas is replaced by PEF, the power consumption of the incubator will be higher than the unaltered shell incubator.

Aside from the power viability, the project has one logistic problem which is the necessity of using one IR camera per incubator. The IR cameras used in this project are expensive due to their high quality and specification. The two presented problems result in higher costs as the price of the incubator, and the maintenance cost increase obviously.

5.2. Discussion: Accuracy of our system over old ones

The current methods used to measure skin temperature require direct skin contact. This implies the placement of a sensor in physical contact with the newborn skin. Thus, touching the newborn and disturbing his/her rest. Besides that, the measured temperature is untrue, because during the measurement the newborn skin suffers conduction, a human thermoregulation function, can affected by which caused by the contact.

The proposed method does not make any kind of invasion into the neonate environment. Additionally, it provides accurate temperature measurement. Furthermore, the innovative method allows a monitoring of skin temperature in real time.
The accuracy which the thermal IR camera has, related to the actual measurement methods is better in one order of magnitude, in numbers it is that actual method which has a 0.5C and the IR camera has 0.05C of accuracy [Jon98, Jor08, Ric04].
Nonetheless, the proposed method is in the prototyping stage, and yet is not considered as a mature clinical monitoring tracking system, i.e., it has some parts unfinished and others to improve. The Image processing software works correctly but has some points that must be considered. Currently, due to the absence of a pseudo-color to temperature conversion table, it is not possible to evaluate the system's accuracy for the measured temperature. Thus, it is not possible to determine the temperature that is measured neither its accuracy. Moreover, the user has to check that the drawn ROI is the exact measurement region, so that the system provides the desired and accurate thermal information.

5.3. Conclusions

This project proposed a new concept to monitor the temperature of a newborn infant and the incubator consequently. As the neonates need the maximum and tolerable control as possible; because they are the most delicate patients and most sensitive for almost tiny temperature gradient or changes inside incubator. The proposed virtual temperature sensor approach, is presents an alternative contactless and non-invasive thermal monitoring against available contact temperature sensing gold standards. The virtual temperature sensing approach will be more reliable and valid temperature monitoring for the NICU units. First proposition which was tested; was to replace a small part of the incubator shell to an IR transparent material, PEF, nevertheless this first proposition is not available as the first discussion exposes. To overcome this problem it is propounded two more possible solutions. The using of the smaller IR camera inside incubator when they will have similar properties (e.g. temperature resolution, IR spectral bandwidth and fast data connectivity) than current IR camera. The other will make a hole in the shell to insert the IR camera.
Moreover, this virtual sensor of skin control temperature for neonate is also able to control baby's breath among other kind of measurements though the baby's movements [AKAL09, Mat09]. For all these facts, it is interesting to continue working on this project [Bla90].
The experiments carried out to calibrate the system provided a lot of results. The obtained data was useful not only to calibrate the camera, but also for two additional uses. The

new method was developed to analyze one material in the infrared spectral range. This method lies on the foundations in the process which is followed to find the material properties in these wavelengths, such as transmittance and reflectance properties. The information about transmittance properties of PEF will be useful in future work and clinical setting implementation. This method can be used in future tests and actually it can improve with more experiments or different approach to perform it.

The developed ROI-tracking software operation is based on the selection of specified image region (measurement region) to the rest of the image and follows this region throughout image. The philosophy behind this project is to stabilizing the measurement ROI during unexpected neonates' involuntary movements. Besides this, the developed software could have a lot of possibilities in the medical thermography imaging, and other temperature process monitoring. Nonetheless, it characterize with some limitations such as, the ROI coordinate stability-profile and the shape-selection of ROI.

The stability problem in the ROI tracking is basically, the differentiation of the ROI from the rest of the image, i.e. against the ROI is more singular in the image, it will be more stable and robust either during relatively stable baby or during involuntary motion takes place simultaneously. Depending on the ROI shape, if the ROI shape is a small and not delineated enough, the software will have difficulty to track the ROI coordinate. On the outlook some upgrade is proposed that it can be solved these problems.

The developed ROI-tracking application was able to detect learned objects of an image, in both situations, moving or still. Due to the versatility of the developed software, small modifications allow it to improve its performance; as well as adequate it to applications for futures investigations.

In the IR image processing chapter, two different acquisition sources were used to test the behaviour of the application. Excepting the acquisition part, the application was maintained in both cases. This proves the application's versatility as it can hold up any kind of image acquisition.

6. Outlook

6.1. Future prospective

In this chapter, it is a series of possible technological upgrades that could be possible in the near future which would help to solve those problems proposed previously.
To solve heat loss problem in the incubator, two possible solutions are proposed. First; is to use compact and miniaturized infrared (IR) thermal cameras to be mounted inside the incubator, and will acquired real-time thermal images without applying any IR-transparent window materials, by which it will affect the calibration result of the IR camera system. This size reduction depends to the IR camera manufacturer and now it is widely produced by several manufactures (e.g. Micro-Epsilon ($\mu\epsilon$) IR camera, or Infratec PIR UC25 camera) as illustrated in figure below.
Hence it is not used as a possible solution for this problem.

Figure 6.1: New compact and miniaturized infrared thermal camera system (a) PIR UC-25 IR camera and (b) Micro-Epsilon ($\mu\epsilon$) IR camera.

The second option is to make a hole in the incubator of the precise dimension so as to fit the IR camera there and in this way a transparent window is not needed and the heat-flow will be maintained inside. In addition, the camera calibration process to compensate temperature variation is not needed. Even though making a hole in the incubator has been carried out, how and where it is made is very important, because there is only one chance.

6.2. Infrared transparent materials improvement

The research made in this project about material transmittance has been really focused into solve the Plexiglas reflectivity problem. The new research direction on IR-optical materials toward and enhancement of infrared transmission properties could optimize the prognosis of

developing medical thermography application.
If this research could be done, more complex research which must use previous research could be focusing in the rest a lot of work is saved for more complex investigations that use this material for infrared frequencies. Such as, in the case if how this work has been done, software applications would be more developed. Hence common material in infrared frequency band research is proposed.

6.3. Improvement of thermal ROI tracking

In the image processing stage; there are many possible improvements alternatives can be applied to the ROI tracking system such as the following:
The first alternative is that; considering the two types of region of interest (ROI). One called the global ROI; which will follow the object, and the other ROI called in some definition (region-of-measurement) (ROM) which will be the one from where the temperature information is extracted. This modification would be very useful. For instance, in the case of the face where mouth, nose, eyes and cheeks move together, the temperature information could be measure for specific facial structures with only one tracked ROI. This tracking application will be faster than current.
The second alternative would be to be able to follow every type of movement of the object. The best image processing would be having it learned once; it would be able to follow all movements, inclusively the out-of-plane rotation. Nonetheless, this requires a high level of image processing that is not known whether LabVIEW can support this process.

A. List of Abbreviations

Symbol	Meaning
AF	Autofocus
AVI	Audio video interleave
$DMTF$	Dynamic-MTF
EM	Electromagnetic
$FLIR$	Forward looking infrared
FOV	Field of view
FPA	Focal plane array
GUI	Graphical user interface
IC	Indurect calorimetry
IR	Infrared
ITC	Infrared thermographic calorimetry
LCD	Liguid crystal display
$LWIR$	Long-wave infrared
MTF	Modulation transfer function
$MWIR$	Middle-wave infrared
$NETD$	Noise equivalent temperature differential
$NICU$	Neonatal intensive-care unit

Symbol	Meaning
$NWIR$	Near-wave infrared
PE	Polyehtylene
PEF	Polyethylene foil
RAM	Random acces memory
RMS	Root meas square
ROI	Region of interest
ROM	Region of measurement
$SITF$	System intensity tranfer function
$SWIRP$	Short-wave infrared
UV	Ultraviolet

B. LabView thermal image processing

This appendix shows the Labview process of all stages in the thermal imaging processing. It is ordered with the same distribution than the explanation about the infrared image processing, i.e. IR acquisition, ROI geometry definition, Tracking object, ROI temperature extraction and Display.

B.1. IR Acquisition

In this stage it is explained the functions that the Labview uses to acquire the image signal. The USB camera and the AVI acquisition are defined in this stage and also their disconnection at the end of the application.
The USB camera acquisition allows the real-time test. This point is useful to know the capacity of the system at real-time.

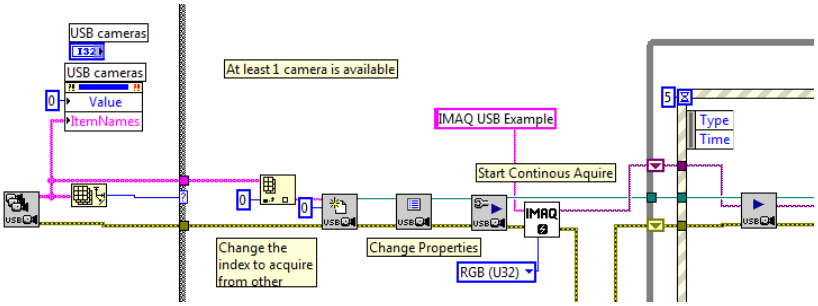

Figure B.1: USB camera acquisition

Figure B.1 shows the LabVIEW block diagram for the communication with the USB webcam. The first block, *IMAQ USB Enumerate Cameras* finds all the connected USB cameras to the laptop and returns an array with USB cameras names. When the resulting array is empty, the application ends. After choosing the first name in the array, the *IMAQ USB Init* creates an *IMAQ USB session* for the specified USB camera. After initializing an *IMAQ USB session*, the *IMAQ USB PropertyPage* launches a configuration dialog box. The box is provided by the camera manufacturer. The next step is *IMAQ USB Grab Setup* that configures and starts a continuous acquisition. Before starting the acquisition, an *IMAQ image reference* is created by the *IMAQ create block*. And the *IMAQ USB Grab Acquire* acquires the image during in the continuous acquisition.

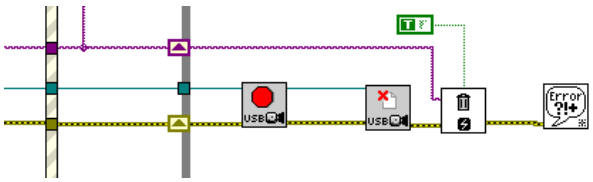

Figure B.2: USB camera disconnection

In figure B.2 it is represented the blocks that end the *IMAQ USB session*. The first block, *IMAQ USB Stop*, stops the continuous acquisition. The next block is the *IMAQ USB Close* which closes the USB camera session, previously opened using the *IMAQ USB Init* VI. The following two blocks are not for USB camera acquisition still they must be used at the end of the application. First is the *IMAQ Dispose* which erases the image and frees the space it occupied in the memory. The LabVIEW requires erasing each created image in an application to free the memory allocated to the *IMAQ Create* VI. In this case, the *IMAQ Dispose* is called just once for all images created with the *IMAQ Create*.
The second block is the *General Error Handler* VI that indicates whether an error occurred. If an error occurred, this VI returns a description of the error and optionally displays a dialog box.
Relatively to the pseudo-color images sequence. The pseudo-color is the color range that represents the temperatures present in IR image. This representation makes it possible for the human eye can to interpret the temperature information. To obtain a sequence from the IR camera is necessary to realize a previous job that consists in transforming a test sequence from IR camera in an AVI format. The first step is record the test sequence which is acquired from an object moving throughout FOV. In this case a person was used as an object, as seen in the figure B.3.

Figure B.3: Extracted images from AVI.

The two pictures in Figure B.3 are an example of images from the test sequence and show the object, a person face, moving throughout the FOV.
When the test sequence was recorded, The IRBIS 3 Professional converted the IRBIS sequence files to AVI video. It was done using the AVI option in Extras menu which is explained in stage 3.2.
To test the behavior of the application with pseudo-color images, the AVI acquisition system and the IR video are combined being the IR-Acquisition block from the application.

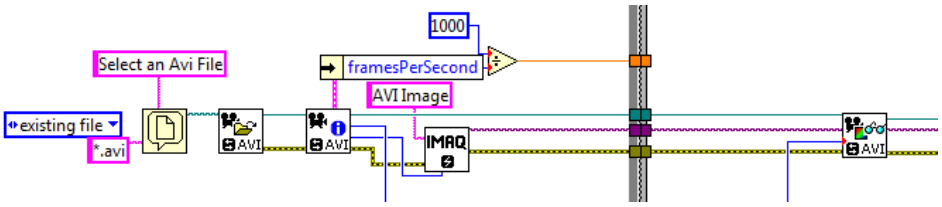

Figure B.4: AVI acquisition

The block diagram in figure B.4 represents the initialization of the video reproduction in LabVIEW. Before starting the acquisition, the user must choose an avi file. This is made using the File dialog that displays a dialog box where the user specifies the path to a file or directory. The *IMAQ AVI Open* opens an existing AVI file from the selected path. The last VI returns an *AVI Refnum* that specifies the opened AVI file. *AVI Refnum* enters in the *IMAQ AVI Get Info* that obtains information about the AVI file associated with *AVI Refnum*. The information consists of Frame data, Number of Frames and Image Type. The latter is used in the *IMAQ Create* so that the image type remains unchanged. Finally, the *IMAQ AVI Read Frame* reads the image from the AVI file specified by *AVI Refnum*.

Figure B.5: AVI disconnection

At the end of the application it is necessary to close the AVI file associated with the AVI Refnum. This is done using the *IMAQ AVI Close* as shown in Figure B.5. Furthermore, the *IMAQ Dispose* and *General Error Handler* VI has the same function as in USB camera acquisition. At the end of the video it is necessary to close the video and image references. The acquisition models for USB camera and AVI have been based in previous models. This helped to develop other parts more deeply.

B.2. ROI geometry definition

The ROI is the specific part of the image from temperature information will be extracted. Its shape is also determined by the user who may choose between rectangular, circular or freehand. Moreover, the program is able to learn a new ROI in any moment and also to make a reset of all ROI previously learned.
The learned ROIs are templates that the tracking will use to localize each ROI inside the image. All templates are saved in a template array which later will be used in the tracking process.

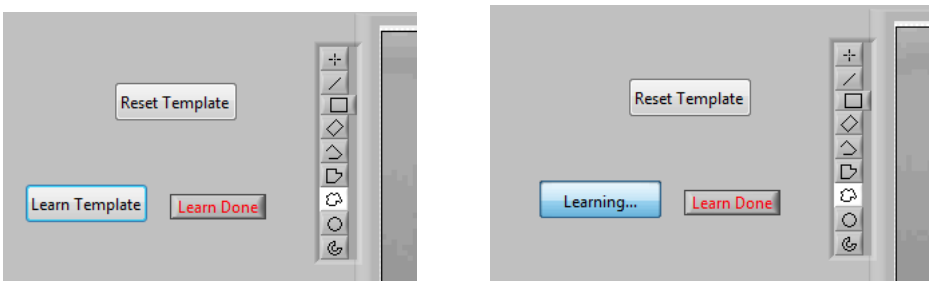

Figure B.6: Learn buttons.

In figure B.6 is shown the process of learning a new template. Firstly, the image is stopped by clicking “Learn Template“. The next step is selecting which kind of ROI is wanted in the options column. After the selection of type of ROI, it is placed in the image part that to be followed, i.e. learned template. When the ROI is chosen, “Learn Done“ is clicked and then image runs normally again. Another option is the RReset Templatetthat deletes all learned templates.

Figure B.7: Draw ROI sample.

Figure B.7 presents a sample of drawn ROI in the image. The sample is a stopped image during the learning mode. The user has unlimited time to draw the new ROI. When the user finishes drawing the ROI, he must click the button "Learn done" to finish the learn mode.

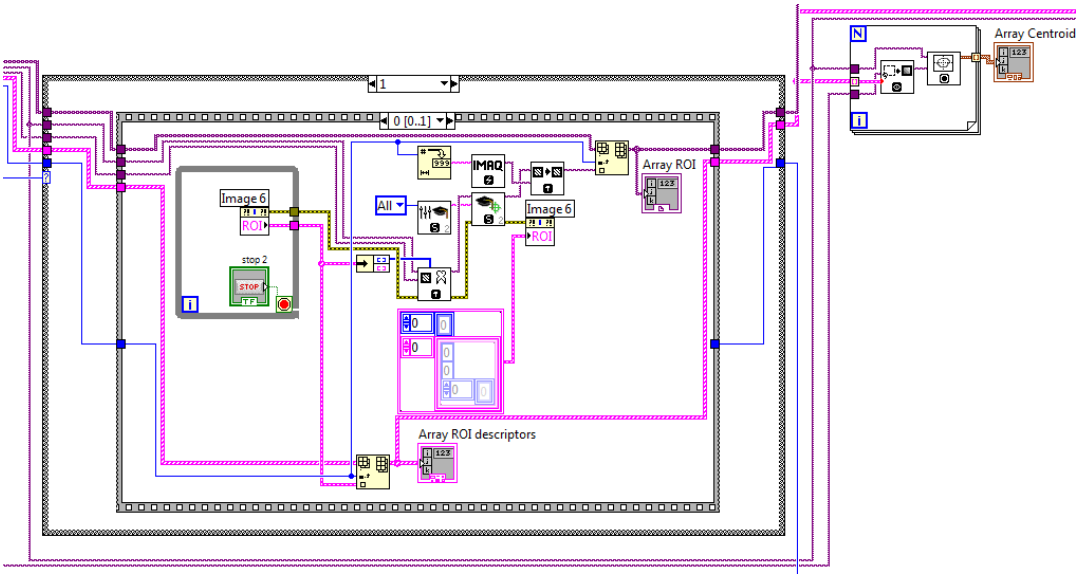

Figure B.8: ROI geometry definition.

The *ROI geometry definition* block diagram has three work modes which are Default, Reset and Learn (see Figure B.8). These modes are activated from Graphical User Interface (GUI) buttons (see Figure B.6). The *Default* mode works with previous parameters. The *Reset* mode deletes all information about learned ROIs, components and ROI Descriptors Arrays.

Finally, the *Learn* mode is the process which runs the application to learn a new ROI. The block diagram is explained as sequential as possible. First of all, the application waits for the definition of the ROI by the user. This is done with a while loop which waits until user click "learn done" in front panel. The first block, the *IMAQ Extract* extracts a part of the image with adjustment of the horizontal and vertical resolution. The *IMAQ Setup Learn Pattern 2* block sets the parameters used during the learning phase. The *IMAQ Learn Pattern 2* creates a description of the template image that the user wants to search. After this template image is attached to ROI array. And the ROI Descriptor from drawn ROI is attached to ROI Description array. Furthermore, the center of each learned ROI is saved to use further along.

B.3. Tracking Object

The most important part of the project application is tracking, in order to find learned ROI in the image.

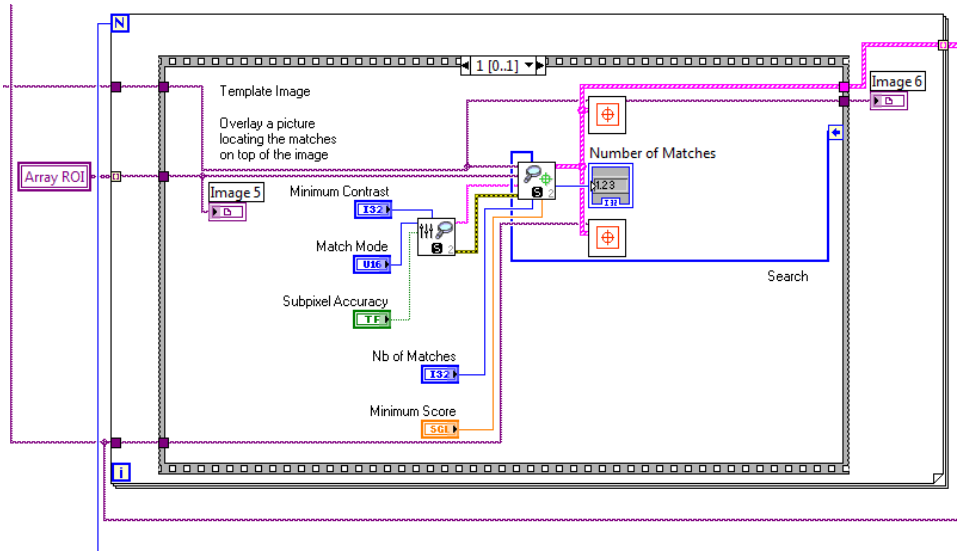

Figure B.9: ROI Tracking.

The block diagram shown in figure B.9 is repeated for each learned ROI. For this reason the loop makes as much iteration as the learned ROIs. This process is continuously running as it is never known which ROI or ROIs are in the image in any moment. The *IMAQ Setup Match Pattern 2* sets the parameters that are used during the matching process. These parameters are Minimum Contrast, Match Mode and Subpixel Accuracy. Minimum Contrast specifies the minimum expected difference between the maximum pixel value and the minimum pixel

value in the image. Match Mode particularizes the invariance mode to use when looking for the template pattern in the inspection image: Shift Invariant searches for the template image, allowing up to 4 of rotation and Rotation Invariant searches for the template in the image regardless of the rotation of the template. And Subpixel Accuracy determines if to return the match results with subpixel accuracy. For this application the parameters' values are 10 of minimum contrast, rotation invariant and subpixel Accuracy is ignored because Match Feature Mode is set to color. Next block is the *IMAQ Match Pattern 2*. This block searches for a template image in an inspection image. The parameters from the *IMAQ Match Pattern 2* are Optional Rectangle, Match Pattern Setup Data, Number of Matches Requested and Minimum Match Score. Optional Rectangle defines a four-element array that contains the left, top, right and bottom coordinates of the region to process. This region is determined by Global Rectangle from ROI descriptor. Match Pattern Setup Data is a string that contains information from the *IMAQ Setup Match Pattern 2* VI. Number of Matches Requested is the number of valid matches expected; this application expects a single match from each ROI in an inspection image. Minimum Match Score is the smallest score a match can have to be considered valid; the considered smallest score is 700. The data range for a match is between 0 and 1000.

The *IMAQ Match Pattern 2* returns Matches and Number of Matches. Matches returns the following elements: Position is a point-coordinate cluster corresponding to the center of the template. Angle is the rotation angle of the template in the source image at the current match location. Scale is the change in percentage size of the matched template from the original template, normally 1. Score ranks the match results on a scale of 0 to 1000, where 0 equals no match and 1000 equals a perfect match. And Bounding Box is an array of five points that define the boundary of the template pattern in the image. Matches is connected directly to the Draw Pattern Matches Position that draws matched rectangles in an inspection image. And Number of Matches is the number of template matches found in the inspection image based on the input settings; this result informs whether ROI are matched in an inspection image.

It is important to notice that the application will work more slowly than it has more findable ROIs. For this reason, the user must learn only the just ROIs. Another problem from much ROI is the inspection time. The inspection time is the every few frames is inspected the image by each ROI. The application couldn't consider a real-time application if the inspection time was so large because it has lost information in this time.

Figure B.10: Sample ROI tracking.

Figure B.10 presents a sample of drawn ROI in an IR sequence. As seen, the application overlays a rectangle in the position where the learned ROI is placed in the inspection image; in this case, the learned ROI is an IR nose in a IR sequence of a face moving into FOV.

B.4. Extract information

The fourth part is the extraction of the relevant information from detected ROI. The information about detected ROI that arrives from Tracking object part is separated to obtain the relevant information about ROI temperature. The information contains the position of ROI center in the image and its shape. After it is extracted all information about ROI, the image part where ROI is placed is separated from the rest of the image. The color information is extracted from isolated image.

At this point the color information of ROI is known. This color information is a pseudo-color from IR camera. This pseudo-color is based in a conversion temperature to color. Then, to transform color information to temperature is necessary to apply inverse transform of color-temperature table. This color-temperature table is given by IR-Acquisition block that knows all about IR image from IR camera. Moreover, a block which shows analyzed image is implemented; it contributes in visual information to the user, but is irrelevant to the process.

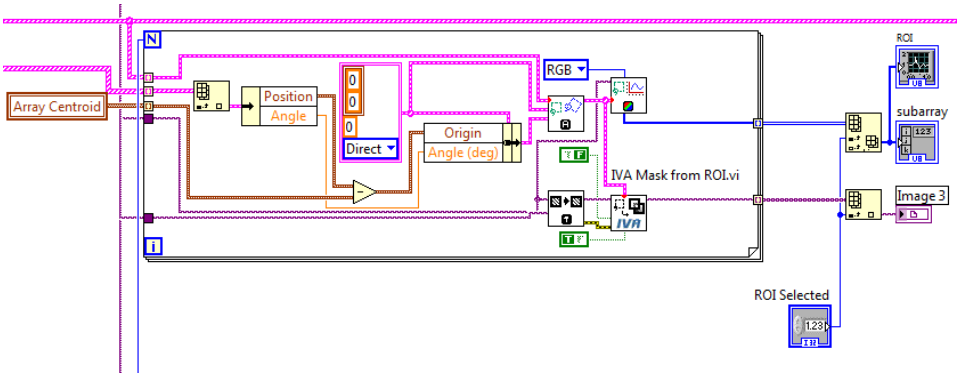

Figure B.11: Extract information.

In Figure B.11, it has some different steps are carried out. The most important part in this process is to select all information for each learned ROI. As all learned ROI must be shown its information, a loop choice in ROI matched information array, ROI description array and Centroid array in order to each iteration that represents each learned ROI like in tracking block.

This block diagram carries out the mathematics operations to isolate the ROI from the rest of the image. As all detected ROI must analyze the color information, this part realizes a for loop to extract all relevant information from each ROI. First at all, Centroid array from ROI geometry definition block diagram, Matches array and ROI Descriptor array are introduced to the loop. The matched ROI's position and angle are separated from the rest information from the Matches information. This position is subtracted the Centroid from respective ROI. This operation is necessary because the given position from Matches is referenced to the ROI center and the ROI Descriptor's position has the reference in the left-top corner of ROI, for this reason is necessary to put all ROI positions in the same coordinate system. After subtract, the new position and angle are placed in a Base reference cluster. All of these operations are made to can modify to new reference the known ROI Descriptor. It is made by the *IMAQ TransformROI* that translates and rotates an ROI in an image to transform the ROI from one coordinate system to another. Base Reference is the base coordinate system; it always is (0, 0) position and 0 angle. New Reference is the new coordinate system; it is the made Base reference with matched ROI's position and angle. The *IMAQ TransformROI* returns a new ROI Descriptor for the transformed ROI. The new ROI Descriptor and the original IR image are introduced in two different blocks that one extracts color data from the ROI and the other shows the isolated ROI. The first of these blocks is the *Get Color Line Profile* that returns three data array with color information about the placed ROI in the image depending for color mode. The Color mode options are RGB (Red, Green and Blue), HSL (Hue, Saturation and Luminance), HSV (Value) and HSI (Intensity). The other block

is the *Mask from ROI* that recopies in the image the pixels inside or outside the ROI and it is possible to shrink the selected image. The returned results of each learned ROI is added to array at the end of the loop.

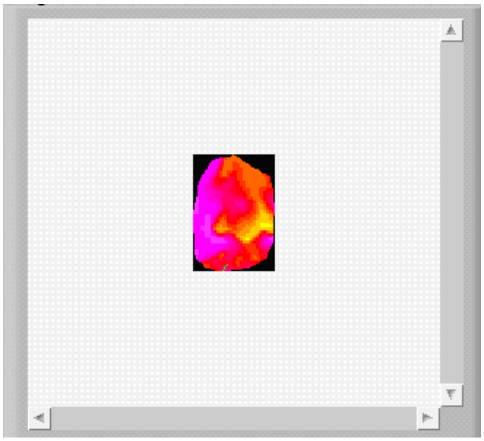

Figure B.12: Extracted ROI from image.

Figure B.12 is a sample of final result of extracted ROI and it is showed in image display; it is the image which is returned by the *Mask from ROI*. This image does not offer temperature information directly, but it is of service to the user to know if the shown ROI is the ROI that the user has chosen in the learning part.

B.5. Display

The last part is presenting the final results. The results are two types, the original IR image from the camera with overlaid ROI and a plot with color level of the selected ROI.

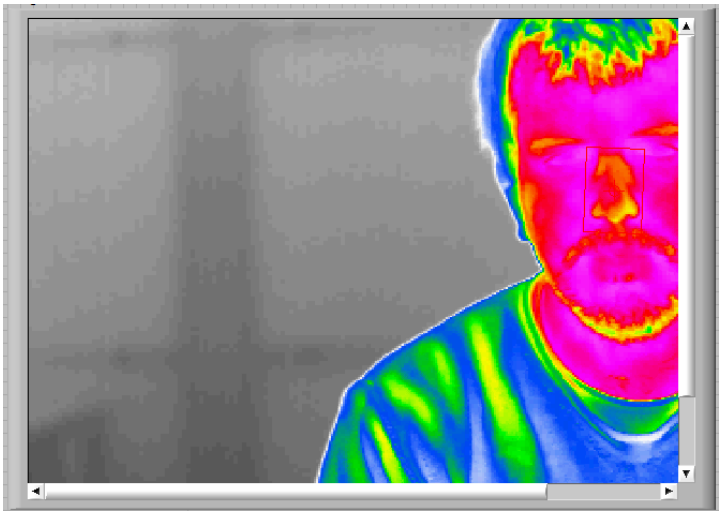

Figure B.13: Showed image with overlaid ROI.

Figure B.13 presents the original image that is provided by IR camera and it is overlaid a rectangle in the ROI place. This rectangle notifies the user where is the tracking ROI. This display is useful to users that can control the good working of the system. The results are showed each ROI individually by ROI selector in a plot, as seen in the figure B.14.

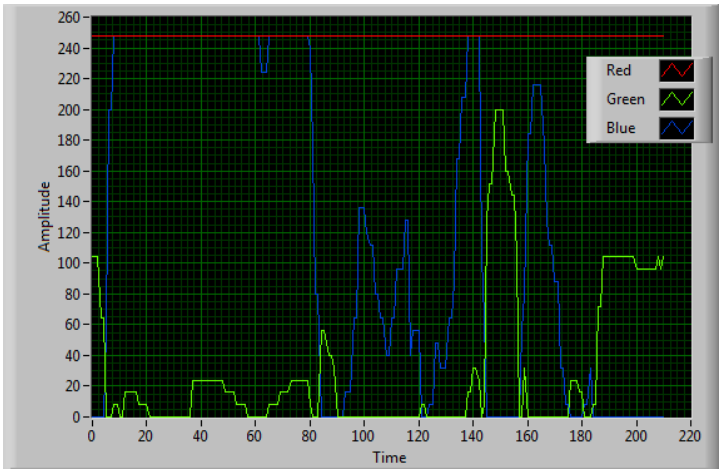

Figure B.14: Color information from localized ROI.

The plot in Figure B.14 displays primary color levels, red, green and blue, from ROI. This color information is useful to determine which temperature has the ROI, which is the aim of the project, scilicet, the virtual sensor of temperature non-contact and non-invasive is made. But the process that transforms color to temperature will be implemented when Acquisition block of IR camera will concrete as possible.

References

[Ada00] R. A.; Bell E. F. & Egoavil C. A. Adams, A. K.; Nelson. Use of infrared thermographic calorimetry to determine energy expenditure in preterm infants. Am J Clin Nutr, 71(4):969–977, 2000.

[AKAL09] Th. Orlikowsky Abbas K. Abbas, K. Heimann and Steffen Leonhadrt. Non-contact respiration monitoring based on real-time infrared thermography imaging. In Olaf Doessel, editor, World conference on Medical Physics and Biomedical Engineering. IFBME, IFBME, 2009.

[AP90] Wailoo M.P. Anderson, E.S. and S.A. Petersen. Use of thermaographic imaging to study babies sleepong at home. Archives of Disease in Childhood, Vol. 65, No 11:pp. 1266–1267, November 1990.

[Bar63] R.B. Barnes. Thermography of the human body. Science Magazine, Vol. 140, No 3569:pp. 870–877, May 1963.

[Bha76] J. R.; Haberman J. D. & Boon D. J. Bhatia, M.; Poley. Abdominal thermography in infantile and childhood liver disease. South Med J, 69(8):1045–1048, 1976.

[Bla90] R. P.; Darton K.; Goff M. R.; Norman T. D. & Spikes H. A. Black, C. M.; Clark. A pyroelectric thermal imaging system for use in medical diagnosis. J Biomed Eng, 12(4):281–286, 1990.

[Can99] J. Caniou. Passive Infrared Detection: Theory and applications. Kluwer Academic Publisher, 1999.

[Cho97] K.; Sagawa S. & Shiraki K. Choi, J. K.; Miki. Evaluation of mean skin temperature formulas by infrared thermography. Int J Biometeorol, 41(2):68–75, 1997.

[Chr03] Heinz; Rosegger Hellfried; Engele Heidi; Kurz Ronald & Kerbl Reinhold Christidis, Iris; Zotter. Infrared thermography in newborns: the first hour after birth. Gynakol Geburtshilfliche Rundsch, 43(1):31–35, 2003.

[Cla80] J. K. Clark, R. P. & Stothers. Neonatal skin temperature distribution using infrared colour thermography. J Physiol, 302:323–333, 1980.

[Cro75] J. K.; Warner R. M. & Woodrough R. W. Cross, K. W.; Stothers. Proceedings: The application of thermography to the detection of energy metabolism of the brain in the new-born infant. J Physiol, 252(2):44P–45P, 1975.

[Dan06] A. Daniels. Field Guide to infrared Systems. SPIE Press, Bellingham, 2006.

[GC94] G. Gaussorgues and S. Chomet. Infrared Thermography. University Press, Cambridge, 1994.

[GDH07] J. Griffiths and J.A. De Haset. Fourier Transform Infrared Spectrometry. Wiley, 2007.

[Ger99] L. Gerward. Paul villard and his discovery of gamma rays. Physics in Perspective, Vol. 1, No 4:pp. 367–383, December 1999.

[GP08] Vizgaitis J. Pellegrino J. G. Grenn, M. W. and P Perconti. Infrared Camera and Optics for Medical Applications, Medical Infrared Imaging. CRC Press, Boca Raton, FL, 2008.

[Hin09] P. H. Hindle. Handbook of Near-Infrared Analysis, Historical Development. CRC Press, Boca Raton, FL, 2009.

[HR02] M. Henini and M Razeghi. Infrared: Detection technologies. Elsevier Advanced Technology, UK, 2002.

[Jia05] E. Y K; Yeo A. C B; Wu S.; Pan F.; Yau W. Y.; Chen J. H. & Yang Y. Jiang, L. J.; Ng. A perspective on medical infrared imaging. J Med Eng Technol, 29(6):257–267, 2005.

[Jon98] B. F. Jones. A reappraisal of the use of infrared thermal image analysis in medicine. IEEE Trans Med Imaging, 17(6):1019–1027, 1998.

[Jor08] A-L.; Dastidar P.; Soimakallio S.; Kuukasjrvi T.; Toivonen T.; Saaristo R. & Jrvenp R. Joro, R.; Lperi. Imaging of breast cancer with mid- and long-wave infrared camera. J Med Eng Technol, 32(3):189–197, 2008.

[Klo91] P. Klocek. Handbook of infrared optical materials. Marcel Dekker, New York, 1991.

[LA03] J.M. Lpez-Alinso. Noise Equivalent Temperature Difference (NETD), Encyclopedia of Optical Engineering. Marcel Dekker, New York, 2003.

[Mat09] S.; Ujikawa K.; Usui T.; Gotoh S.; Sugamata M.; Badarch Z. & Abe S. Matsui, T.; Suzuki. Development of a non-contact screening system for rapid medical inspection at a quarantine depot using a laser doppler blood-flow meter, microwave radar and infrared thermography. J Med Eng Technol, 33(5):403–409, 2009.

[Mer06] G. L. Merla, A. & Romani. Functional infrared imaging in medicine: a quantitative diagnostic approach. Conf Proc IEEE Eng Med Biol Soc, 1:224–227, 2006.

[Mou95] R.F. Mould. Invited review: Rntgen and the discovery of x-rays. British Journal Radiology, Vol. 68, No 815:pp. 1145–1176, November 1995.

[MP50] Dicke R.H. Montgomery, C. G. and E. M. Purcell. Principles of microwave circuits,. McGraw-Hill, London, UK, 1950.

[Pom77] R. L. & Ukrainski C. T. Pomerance, J. J.; Lieberman. Neonatal thermography. Pediatrics, 59(3):345–351, 1977.

[Rel04] C.G. Relf. Image Acquisition and Processing with LABVIEW. CRC Press, FL, 2004.

[Ric04] George R; Douillet Christelle D; Listwa Todd M; Robinson William P; Zarzaur Ben L; Pearlstein Robert & Katz Laurence M Rich, Preston B; Dulabon. Infrared thermography: a rapid, portable, and accurate technique to detect experimental pneumothorax. J Surg Res, 120(2):163–170, 2004.

[RJ08] F. E. Ring and F. Jones, B. The Historical Development of Thermometry and Thermal Imaging in Medicine, Medical Infrared Imaging. CRC Press, Boca Raton, FL, 2008.

[Ryl72] H. & Lind J. Rylander, E.; Pribylov. A thermographic study of infants exposed to cold. Acta Paediatr Scand, 61(1):42–48, 1972.

[SD09] S. Silbernagl and A. Despopoulos. Thermal Balance and Thermoregulation, Color Atlas of Physiology. Thieme Publisher, New York, 2009.

[Wil98] T. L Williams. The Optical Transfer Function of Imaging System. CRC Press, FL, 1998.

[Wil03] K. Wilhelm. Past and recent observations of the solar upper atmosphere at vacuum-ultraviolet wavelengths,. Journal of Atmospheric and Solar-Terrestrial Physics,, Vol. 65, No 2:pp. 167–189., January 2003.

[Wil09] T. L Williams. An Introduction to Thermal Imaging, Thermal Imaging Cameras,. CRC Press, FL, 1st edition, 2009.